Arabian Journal of Chemistry (2023) **16**, 105010

King Saud University

Arabian Journal of Chemistry

www.ksu.edu.sa
www.sciencedirect.com

ORIGINAL ARTICLE

Photocatalytic antimicrobial and photostability studies of TiO_2/ZnO thin films

Endrika Widyastuti [a], **Chen-Tien Chiu** [b], **Jue-Liang Hsu** [c], **Ying Chieh Lee** [d,e,*]

[a] *Department of Food Science and Biotechnology, Faculty of Agricultural Technology, Universitas Brawijaya, Malang 65145, Indonesia*
[b] *Kaohsiung Veterans General Hospital, Kaohsiung City 813414, Taiwan*
[c] *Department of Biological Science and Technology, National Pingtung University of Science and Technology, Pingtung 91201, Taiwan*
[d] *Institute of Precision Electronic Components, National Sun Yat-sen University, Kaohsiung 804, Taiwan*
[e] *School of Dentistry, Kaohsiung Medical University, Kaohsiung 807, Taiwan*

Received 29 March 2023; accepted 13 May 2023
Available online 19 May 2023

KEYWORDS

Antimicrobial coating;
Thermal Oxidation;
TiO_2/ZnO thin films;
Irradiation time

Abstract A nanothin film-based antimicrobial coating has been attractive in response to the rise and spread of pathogenic microbes, which led to the development of low-cost, effective, and rapid disinfection methods for coating material. TiO_2/ZnO bilayer thin films have been developed through magnetron sputtering and thermal oxidation. The influence of oxidation temperature on structural, optical, photocatalytic, photostability, and antimicrobial properties of Ti/ZnO thin films has been addressed. X-ray diffraction (XRD) analysis has shown the presence of hexagonal wurtzite ZnO, $Ti_{0.895}O_{.77}$, and anatase TiO_2 in the bilayer films. Increasing the oxidation temperature reveals a certain degree of crystallization and transforms $Ti_{0.895}O_{.77}$ into the anatase/rutile TiO_2 phase. The bottom layer of ZnO provides sufficient oxygen to improve TiO_2 crystallinity and prevent transforming anatase to rutile during thermal oxidation process. Moreover, Ti/ZnO thermally oxidized at 550 °C exhibit excellent photocatalytic performance under UV irradiation with high photostability. The inhibition rate increased ($p < 0.05$) with irradiation time for *E. coli*, *S. aureus*, and *C. albicans* with effectiveness values reaching approximately 97 ± 3.408, 98 ± 2.409, and 95 ± 3.105 %, respectively. This work reveals that magnetron sputtering through a thermal oxidation approach could generate stellar TiO_2/ZnO thin films as photocatalysts and antimicrobial agents with cost-effectiveness and efficiency.

* Corresponding author.
E-mail addresses: endrika_w@ub.ac.id (E. Widyastuti), ctchiu9393@vghks.gov.tw (C.-T. Chiu), jlhsu@mail.npust.edu.tw (J.-L. Hsu), yc56@mail.nsysu.edu.tw (Y. Chieh Lee).

Peer review under responsibility of King Saud University.

Production and hosting by Elsevier

https://doi.org/10.1016/j.arabjc.2023.105010

1. Introduction

The emerging spread of pathogenic microbes in daily life is raising concerns due to their significant impacts on human health. To counteract this, the development of novel materials such as antimicrobial coatings that prevent the transmission of pathogens has gained traction. These coatings deactivate microorganism effectively on various surfaces, offer high efficiency, provide long-lasting durability, and has no adverse effects (Ahmed et al., 2022; Parfenova et al., 2022; Selvamani et al., 2022; Sheridan et al., 2022). Notably, nanomaterials like ZnO and TiO_2 have garnered considerable attention as antimicrobial coatings due to their excellent photocatalytic activity, low toxicity, and being generally recognized as safe (GRAS) by the US Food and Drug Administration (Azizi-Lalabadi et al., 2019; Nouasria et al., 2022; Phuinthiang et al., 2021). The incorporation of ZnO and TiO_2 materials has been able to enhance photocatalytic activity and antimicrobial properties due to more effective charge separation, higher endurance of charge carriers, and increased interfacial charge transfer to absorbed substrates (Lachom et al., 2017; Pérez-González and Tomás, 2021; Tekin et al., 2020). Moreover, this approach holds great promise for future antimicrobial applications.

Numerous studies have explored the application of ZnO-TiO_2 composites to enhance antibacterial properties (Ali et al., 2021; Dhanalakshmi et al., 2013; Siwińska-Stefańska et al., 2019; Tajdari et al., 2020). The antimicrobial effect of these composites could be attributed to three main factors. Firstly, the release of Zn^{+2} ions by ZnO during characteristic wavelength light absorption causes destruction and disintegration of the bacterial membrane (Pasquet et al., 2014). Secondly, the electrostatic interaction between ZnO or TiO_2 and the microbe cell wall promotes instability of the microbes' membrane (Zhang et al., 2008). Finally, the formation of reactive oxygen species (ROS) on TiO_2/ZnO through light irradiation (Nagvenkar et al., 2016), increases the oxidation of the cellular membrane, thereby enhancing its permeability and decomposition (Szeto, 2006).

Pang et al. (Pang et al., 2019) have achieved significant antibacterial activity against *E. coli* and *S. aureus* using TiO_2/ZnO composite coatings, with deactivation rates reaching to 89.6 and 99.5%, respectively, under 12 h photocatalyst contact time. Moreover, the alignment of ZnO-TiO_2 nanorods reduced the growth of *E. coli* by 40% with a 4-hour contact time. To decrease contact time, Ton et al. (Ton et al., 2020) incorporated ZnO-TiO_2 thin films with a UVB lamp, which successfully inhibited *E. coli* growth by 92.7% in less than 60 min. It is noted that combined UV irradiation lamp and photocatalyst could enhance the microbial killing efficiency. However, no studies have targeted the effectiveness of photocatalyst irradiation time to promote time-effective microbial disinfection. Furthermore, rapid irradiation time exposures should have efficient disinfection and a massive photocatalyst process.

The magnetron sputtering technique has gained attention for large-scale production of ZnO-TiO_2 thin films due to its excellent substrate adhesion and standardized thickness (Güzelçimen et al., 2020; Pérez-González and Tomás, 2021; Suo et al., 2019).However, the use of oxygen as a reactive gas to produce metal oxide film during reactive sputtering could increase production costs. In contrast, the thermal oxidation approach provides a simpler, efficient, and cost-effective method than reactive sputtering for the oxide surface growth of Zn and Ti to form ZnO and TiO_2, respectively (Mihailova et al., 2013; Yeh et al., 2004).

Several studies have investigated the formation of ZnO and TiO_2 films via thermal oxidation of sputtered metal films (Astinchap et al., 2017; Bouanane et al., 2016; Widyastuti et al., 2022; Yeh et al., 2004). The temperature of thermal oxidation influences the TiO_2 phases, which exhibit different levels of photocatalytic activity (Munguti and Dejene, 2020). ZnO's crystalline quality and orientation also have a substantial reliance on the thermal oxidation temperature (Widyastuti et al., 2022). Lee et al. (Lee et al., 2021) reported that the phase structure evolution of a bilayer thin film is significantly affected by oxygen diffusion from the bottom layer during thermal oxidation. Therefore, ZnO film as the bottom layer on Ti/ZnO thin films potentially promotes oxygen diffusion for Ti thin films through thermal oxidation, which is essential for enhancing several thin film properties. By using covered TiO_2 as an upper layer could minimize the effect of photocorrosion on ZnO thin films (Butalid et al., 2020). Photocorrosion that cause dissolution into Zn^{2+} ions of which lead to the loss of photocatalytic material reduces photocatalytic activity and limits its reusability (Sapkal et al., 2012). However, no studies have been reported utilizing the thermal oxidation method to develop TiO_2/ZnO bilayer thin films.

The novelty of this study was the development of TiO_2/ZnO bilayer thin films using magnetron sputtering combined with the thermal oxidation process. This approach aimed to enhance the photocatalytic and antimicrobial activities with effective irradiation time. Hence, this study investigated the crystalline behavior, microstructures, optical, photocatalytic, and photostability properties of TiO_2/ZnO thin films under various oxidation temperatures. Antimicrobial activity of TiO_2/ZnO bilayer thin films against gram-negative, positive bacteria, and pathogenic fungi was evaluated during different irradiation times to determine the effective disinfection time. Therefore, the development of bilayer thin films as an antimicrobial coating is expected to effectively reduce microbial loads and provide a meaningful way to enhance the applications of TiO_2/ZnO thin films.

2. Material and methods

2.1. Materials

Pure Zinc (Zn, 99.99%) and Titanium metal (Ti, 99.99%) as the target material for thin films development was obtained from Ultimate materials Technology Co., Ltd, Taiwan. Glass (FEA Microscope slides) with a 76 × 25 mm dimension was used as a substrate. Argon (Ar, 99.9999%, Xinguang Co., Taiwan) was used in the sputtering process as an inert gas. Acetone (CH_3COCH_3, 95%) and ethanol (C_2H_5OH, 95%) were supplied by Jingming Chemical Co.,Ltd, Taiwan. Methylene blue (MB) (Alfa Aesar; Thermo Fisher Scientific, UK) was used for photocatalytic analysis. The culture collection of *Escherichia coli* ATCC25922, *Staphylococcus aureus* ATCC10234, and *Candida albicans* ATCC10234 as pathogenic microbes was obtained from the Department of Biological Science and Technology, NPUST. Sodium chloride (NaCl), potassium chloride (KCl), sodium phosphate dibasic (Na_2HPO_4), and potassium phosphate monobasic (KH_2PO_4) as the chemicals for producing phosphate buffered saline (PBS) solution were purchased from Sigma-Aldrich, USA. Tryptic soy agar (TSB, DIFCO™), potato dextrose agar (PDA, DIFCO™), Mueller Hinton II agar (MH, BBL™) (from Becton, Dickinson, and Company, USA), yeast extract (Pronadisa, Lab. Conda, Spain), and meat peptone (STBIO Media Inc, Taiwan) were used as microbe growth media. Antibiotics as a positive control in antimicrobial analysis such as Kanamycin, Ampicillin, and Amphotericin-B were also obtained from Sigma-Aldrich, USA). The disk paper (Whatman, Schleicher & Schuell, US) with a 6 mm diameter was used for antibiotic-paper assay procedures. Deionized (DI) water generated by a PURELAB water purification system (Lane End, High Wycombe, UK) was used in all experiments and chemical solution preparation.

2.2. Synthesis of TiO_2/ZnO thin films

The TiO_2/ZnO thin films were developed on a glass substrate using a four-step process. Initially, Zn films were deposited on the glass substrate via magnetron sputtering. Before use, the glass substrates were ultrasonically washed for 30 min each in acetone, ethanol, and distilled water. Moreover, the Zn was then thermally oxidized to produce ZnO from the metallic Zn thin film layer. Furthermore, ZnO thin films were covered with a Ti layer by magnetron sputtering. Finally, thermal oxidation transformed Ti/ZnO thin films into TiO_2/ZnO. As comparative samples, TiO_2 and ZnO thin films were also produced.

The ZnO thin films were prepared by High Power Impulse Magnetron Sputtering (HiPiMS) through thermal oxidation, and their synthesis route has been described in our previous studies (Widyastuti et al., 2022). Direct-current (DC) magnetron sputtering methods with a pure Ti target were used to develop Ti films as an upper layer on ZnO films. The distance between the target and substrate was set at 100 mm. The base pressure was controlled at 1×10^{-6} Torr, and the working pressure was 2×10^{-3} Torr. The argon gas flow is controlled at 6 sccm by mass flow controllers. The substrate holder was rotated at 24 rpm (revolutions per minute). Ti-upper layer films were deposited on ZnO-bottom layer films at 25 °C. The DC power was fixed at 100 W with a 20 min deposition time. The Ti film upper layer thickness was controlled at about 100 nm.

The different oxidation temperatures at 400, 450, 500 and 550 °C for 3 h in the presence of air were designated "Ti/ZnO 400", "Ti/ZnO 450", "Ti/ZnO 500" and "ZnO 550", respectively. For comparison, as references, the Zn and Ti single-layer thin films were oxidized at 400 °C and 500 °C, respectively.

2.3. Characterization of TiO_2/ZnO thin film

X-ray diffraction analyses were performed employing a Bruker D8 Advance model (Germany) with Cu Kα radiation (λ = 1.54). The instrument devices were operated at 40 kV and 40 mA, respectively. XRD analysis for 20 mins scans was continuously performed in a $10° \leq 2\theta \leq 60°$ range, with a step size of 0.1° and a 5 s step size. The International Centre for Diffraction Data (ICDD) card is used for phase identification of crystalline phases in various films. The full width at half maximum (FWHM) value was used to estimate the crystalline size using Scherer's formula. Moreover, the a and c lattice parameters and the total unit cell volume lattice were also calculated **(Supplementary Material A)**.

Field-emission transmission electron microscopy (FE-TEM; FEI Tecnai G2 F20, FEI Company—, USA) was used to observe thin-film cross-section images. Sample preparation for the TEM was performed using a Focused Ion Beam (FIB) (Hitachi NX2000, Hitachi High-Tech, USA). Selected area electron diffraction (SAED) was analyzed using Gatan Software Digital Micrograph software version 3.7.4 (Gatan Inc., USA).

The optical characteristic of thin-film samples, including absorbance and transmittance analysis, were measured using a UV– vis spectrophotometer (U-3310, Hitachi Ltd., Japan) across the wavelength ranges of 200–1000 nm and 300–800 nm, respectively. The optical absorbance was used to measure the thin films band gap using Tauc's equation (**Eq. (1)**): (Singh and Chakrabarti, 2013)

$$\alpha h\nu = A\left(h\nu - E_g\right)^n \tag{1}$$

Where α is the absorption coefficient, $h\nu$ is absorbed photon energy; A is a characteristic parameter independent of photon energy, E_g is the optical energy gap, $n = 2$ for permitted indirect transition, and n = 0.5 for permitted direct transition.

2.4. Assessment of photocatalytic degradation performance of TiO_2/ZnO thin films

A degradation methylene blue (MB) solution with an initial concentration (C_0) of 10 mg/L was used to evaluate the photocatalytic performance of the thin-film samples. Prior to degradation studies, MB solutions with concentrations ranging from 1 to 10 ppm were produced. The calibration equations were derived by linear regression using the intensity (664 nm) displayed for each concentration. Furthermore, the calibration equation was employed to determine the concentration of MB during photocatalytic studies. A 10 ml aqueous MB solution was used to soak thin-film samples, then held under dark conditions for 60 min to create MB absorption equilibrium on the photocatalysts ($t = 0$ min). Photo-irradiation was performed using five commons of UVA lamp tubes (Philips TUV-8-watt, 365 nm, Netherlands) and placed horizontally inside an artificial box. Thin films were retained at 9 cm from the UV light. The photocatalytic activity of thin-film samples was investigated by decomposition of Methylene Blue (MB) solution under UVA irradiation. The concentration of MB in the solution was measured every 30 min for 5 h (t = 30–300 min, C_{30} to C_{300}), and the changes in the MB absorbance were analyzed using UV– vis spectrophotometer (U-3310, Hitachi Ltd., Japan) (Lee et al., 2021). The degradation performance was calculated using equation (**Eq. (2)**): (Lee et al., 2021)

$$\textit{Methylene Blue Degradation}(\%) = \left[1 - \left(\frac{C_t}{C_0}\right)\right] \times 100 \tag{2}$$

Where C_0 is the initial concentration of MB and C_t is the absorbance after different time intervals. The detailed schematic diagram of photocatalytic set up was shown in Fig. 1.

The photostability analysis of thin films for five-cycle reusability was investigated. After the first photocatalytic treatment was finished, thin film samples were detached, rinsed with distilled water several times, air-dried, and placed in a new MB solution. The next step repeats as described previously. The degradation performance was deliberated by each cycle using **Eq. (2)**.

2.5. Assessment of antimicrobial activity performance

Two different assays (qualitative and quantitative) were carried out to investigate thin-film samples' antibacterial and antifungal activities. In this study, *Escherichia coli*, *Staphylococcus aureus,* and *Candida albicans* were used as models for gram-negative, gram-positive, and pathogenic fungi (Table 1). The detailed microbial preparation was followed by a previous study (Widyastuti et al., 2022). Different media were used to enhance bacteria and fungi, which were then cultured aerobically on a rotary shaker for 18–24 h. The PBS solution was

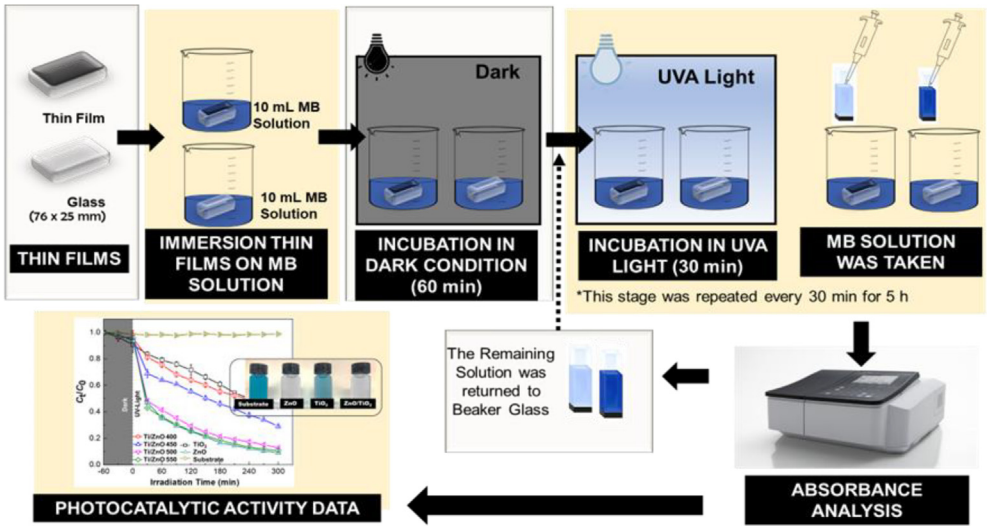

Fig. 1 Schematic presentation of photocatalytic set-up.

then used to collect, wash, and re-suspend the cells. Thin-film samples and glass were cut at 1 cm × 1 cm to evaluate the antimicrobial properties. Three types of antibiotics, Kanamycin, Ampicillin, and Amphotericin-B were used as positive control treatments for *E. coli*, *S. aureus*, and *C. albicans*, respectively.

2.5.1. The agar diffusion method

The final concentration of bacteria and fungi at 10^7 and 10^9 colony-forming units per mL (CFU/mL), respectively, were chosen for agar diffusion methods. 100 µL of each microbe suspension was spread on Muller-Hinton agar plates. The sterile disk paper was used to be impregnated with different antibiotics (positive control). Then, 10 µL of antibiotic was dispended onto the disk's surface. All the samples were gently placed over the seeded agar. Furthermore, to observe the influence of light conditions on antimicrobial activity, the agar plates were exposed to a UVA lamp (8 W, Philips TUV), visible lamp (8 W, Philips T5), and absence of light (dark) conditions for 30 min at room temperature (25 ± 2 °C). After 30 min, the plates were incubated for 24 h at 37 °C. The antimicrobial activity was measured from the diameter (mm) of the inhibition zone. All the experiments were conducted in a sterile environment.

Table 1 Particulars of examined microbe, growth media, and antibiotic treatment as a positive control.

Microbe	Type	Growth Media	Positive Control (concentration)
Escherichia coli	gram-negative	Tryptic Soy agar (TSA)	Kanamycin (100 µg/mL)
Staphylococcus aureus	gram-positive	Tryptic Soy agar (TSA)	Ampicillin (100 µg/mL)
Candida albicans	fungi	Yeast Extract-Peptone-Dextrose (YPD)	Amphotericin-B (10 µg/mL)

2.5.2. The agar dilution method

Antimicrobial analysis using agar dilution methods was studied by the addition of 40 µL of microbes (10^5 CFU/mL) to the sample surface placed on sterilized cell culture plates. Plates were sealed before being exposed to UVA light conditions at room temperature (25 ± 2 °C). All the samples were applied to different UVA irradiation times (10, 20, and 30 min). At various irradiation time intervals, the remaining sample solution on thin-film samples was taken, and serial dilution was performed. Furthermore, the solution was directly spread uniformly onto culture agar plates and incubated at 37 °C for 24 h. After incubation, the numbers of colonies present in the plates were counted using the equation: **(Eq. (3))** (Widyastuti et al., 2021):

$$\boldsymbol{MicrobialInhibition} = [1 - \left(\frac{\boldsymbol{CFUtreated}}{\boldsymbol{CFUcontrol}}\right)] \times 100\% \quad (3)$$

An initial or beginning concentration of microbes (CFU/mL) is known as CFU control, while an irradiated (UV) concentration of microbes is known as CFU treatment. To ensure the accuracy of the findings, each experiment was performed in triplicate.

2.6. Statistical analysis

The quantitative data was conducted in three replicates and analyzed using One-way analysis of variance (ANOVA) by Tukey HSD tests at a $p < 0.05$ significance level in SPSS Statistics version 16 software (SPSS for Windows; IBM Corp, USA).

3. Results and discussion

3.1. Structural analysis of TiO_2/ZnO bilayer thin films

The X-ray diffraction patterns (XRD) analysis was employed to determine the crystal phase of ZnO, TiO_2, and TiO_2/ZnO bilayer thin films. The XRD pattern for Ti, Zn as a single layer, and Ti/ZnO bilayer thin films thermally oxidized at

400 °C are shown in Fig. 2**a**. The sputter-deposited single-layer Zn thin films were metallic and transparent when thermally oxidized at 400 °C with intensity diffraction peaks corresponding to hexagonal wurtzite zinc oxide (ZnO) (hexagonal, space group: *P*63mc, ICDD Card No. 36–1451). However, the pure Ti sample does not exhibit any peaks that only manifest the presence of an amorphous phase. Comparatively, the crystal phase of Ti/ZnO, when thermally oxidized at 400 °C, the TiO_2 rutile (tetragonal, space group = *P*42/mnm, ICDD Card No. 21–1276) and anatase phase (body-centered tetragonal; space group = *I*41/amd, ICDD Card No. 89–2809), $Ti_{0.895}O_{.77}$ (Face-centered cubic, space group: Fm-3 m, ICDD Card No. 89–3075) and ZnO phases appeared. The non-stoichiometry $Ti_{0.895}O_{.77}$ phases attributed to TiO_2 have insufficient oxygen during thermal oxidation, and this layer exists between the upper and the bottom layer. It is demonstrated that appearing a ZnO as the bottom layer could provide sufficient oxygen to the Ti upper layer during the thermal oxidation process. Lee et al. (Lee et al., 2021) reported that oxygen diffusion from the bottom layer significantly affects the film's phase structure evolution. Therefore, it is believed that the phase evolution effects on the Ti films oxidized using thermal oxidation depend strongly on the bottom layer. Previous studies demonstrated that the ZnO layer improved the crystallinity of the TiO_2 thin film (Hussin et al., 2019).

A further increase in temperature to 500 °C resulted in increased diffraction intensity with a decrease in the amorphous background, indicating improved Ti film crystallinity as a single layer and TiO_2/ZnO bilayer thin film, as presented in Fig. 2**b**. Anatase and rutile phases were observed on both samples. This result demonstrated that increasing thermal oxidation temperature increased anatase and rutile peak intensity. It was reported that the temperature and time of heat treatment were found to enhance the crystallization degree and growth rate of ZnO and TiO_2 (Munguti and Dejene, 2020). In addition, the TiO_2 and ZnO thin films develop during the layer-by-layer sputtering process exhibit good contact, ensuring that the TiO_2/ZnO thin films possess a good heterojunction structure (Ton et al., 2020).

In order to determine the effect of oxidation temperature on the bilayer thin films, the Ti/ZnO thin films were thermally oxidized from 400 to 550 °C for 2 h (Fig. 3**)**. Temperature conditions highly influenced the crystallinity during the thermal oxidation process. Increases oxidation temperature on TiO_2/ZnO thin films will transform $Ti_{0.895}O_{.77}$ to anatase/rutile TiO_2 phase. Moreover, the peak of (1 1 0), (1 0 1), (1 1 1), and (2 1 1) orientations of the rutile TiO_2 structure increases considerably during the thermal oxidation process. It is well known that the anatase is a *meta*-stable phase that may be transformed into a rutile phase during heat treatment (Zhou et al., 2013a). Interestingly, the anatase phase still possesses, although oxidation temperature increased to 550 °C. It demonstrates that surface modification with ZnO on bilayer thin films can effectively inhibit the phase transformation from anatase to rutile, which is favorable to improving anatase thermal stability. Similar results were reported by Jing et al. (Jing et al., 2009), which showed that modified Bi_2O_3 species on TiO_2 nanoparticles could improve the thermal stability of anatase crystallites and promote photoinduced charge separation. Further study of the microstructure using Transmission Electron Microscopy (TEM) will be performed to prove the phases existences.

The TiO_2 and ZnO thin films' crystallinity may be improved by reducing the diffraction peak's full width at half maximum (FWHM) as the oxidation temperature rises (Rusu et al., 2007). The result is in accordance with earlier studies of ZnO-TiO_2 composites prepared by different heat treatments such as calcination and annealing temperature (Munguti and Dejene, 2020). The Ti atoms in the films could absorb and/or absorb the O_2 in the air during thermal oxidation of the film. The atoms of Ti and O receive sufficient free energy simultaneously to assist in the nucleation, growth, and aggregation of crystal grains. (Zhou et al., 2013a). According to Perez-Gonzales et al.(Pérez-González et al., 2015), the introduction of ZnO to TiO_2 causes the removal of the anatase phase. Similarly, it has been discovered by other researchers that the anatase phase of TiO_2 may reduce by increasing the quantity of ZnO (Chen and Xu, 2014).

The crystallite size and lattice constants of the ZnO, TiO_2, and bilayer thin films are estimated using the Debye-Scherrer and Bragg's equation, respectively **(Supplementary Material A)**, from the (0 0 2) peak for ZnO and from the (1 1 0) peak for TiO_2. These peaks are chosen since they are relatively intense peaks in the recorded XRD spectrum. The calculated crystalline size (D), lattice parameter ZnO, TiO_2 as a single layer, and bilayer thin films are summarized in Table 2**.**

The average of crystallites ranged between 7.356 and 26.541 nm (Table 2). It was found that by employing thermal oxidation procedures, this research achieved TiO_2/ZnO bilayer thin films with crystallite sizes smaller than those previously reported by means of sol–gel (Lachom et al., 2017) and reactive-magnetron sputtering (Ton et al., 2020) that was earlier reported. The evidence clearly indicates that Ti/ZnO O_2, through thermal oxidation, can promote decreasing crystalline size. A photocatalyst with smaller crystal size and a high specific surface area has more specific reaction sites accessible to undertake photocatalytic reactions, which plays a fundamental role in increasing the photocatalytic performance (Pérez-González and Tomás, 2021).

Therefore, the crystallite size of ZnO and TiO_2 on TiO_2/ZnO bilayer thin film was also affected by increasing oxidation temperature. The higher mobility of atoms, which tend to migrate to the most stable in the lattice, may explain the increases in crystallite size with increasing oxidation temperature (Ayana et al., 2022) and small grains fused collectively to increase grain size (Ibrahim et al., 2013). However, the sample oxidized at 400 °C exhibited the smallest crystallite sizes, resulting from poor crystallization. A rise in oxidation temperature increased crystallite development up to 500 °C, where a decrease was observed. It could be seen that the grain size of the films oxidized 500 to 550 °C decreases from 16.251 to 11.514 nm and 26.541 to 24.159 nm for TiO_2 and ZnO, respectively. A similar trend was also reported by Munguti et al. (Munguti and Dejene, 2020), Mragui et al. (El Mragui et al., 2019), and Khan et al. (Khan et al., 2018). Wittawat et al. (2020) suggested that the crystal size of ZnO and TiO_2 decreased while the temperature increased from 400 °C to 600 °C due to an increasingly high nucleation rate (Wittawat et al., 2020). The results revealed that oxidation temperature is essential in crystal structure formation and crystallite size control.

The effect of oxidation temperature on the microstructure of TiO_2/ZnO bilayer thin films was confirmed using High-resolution TEM (HR-TEM). Fig. 4**a** shows the bright cross-

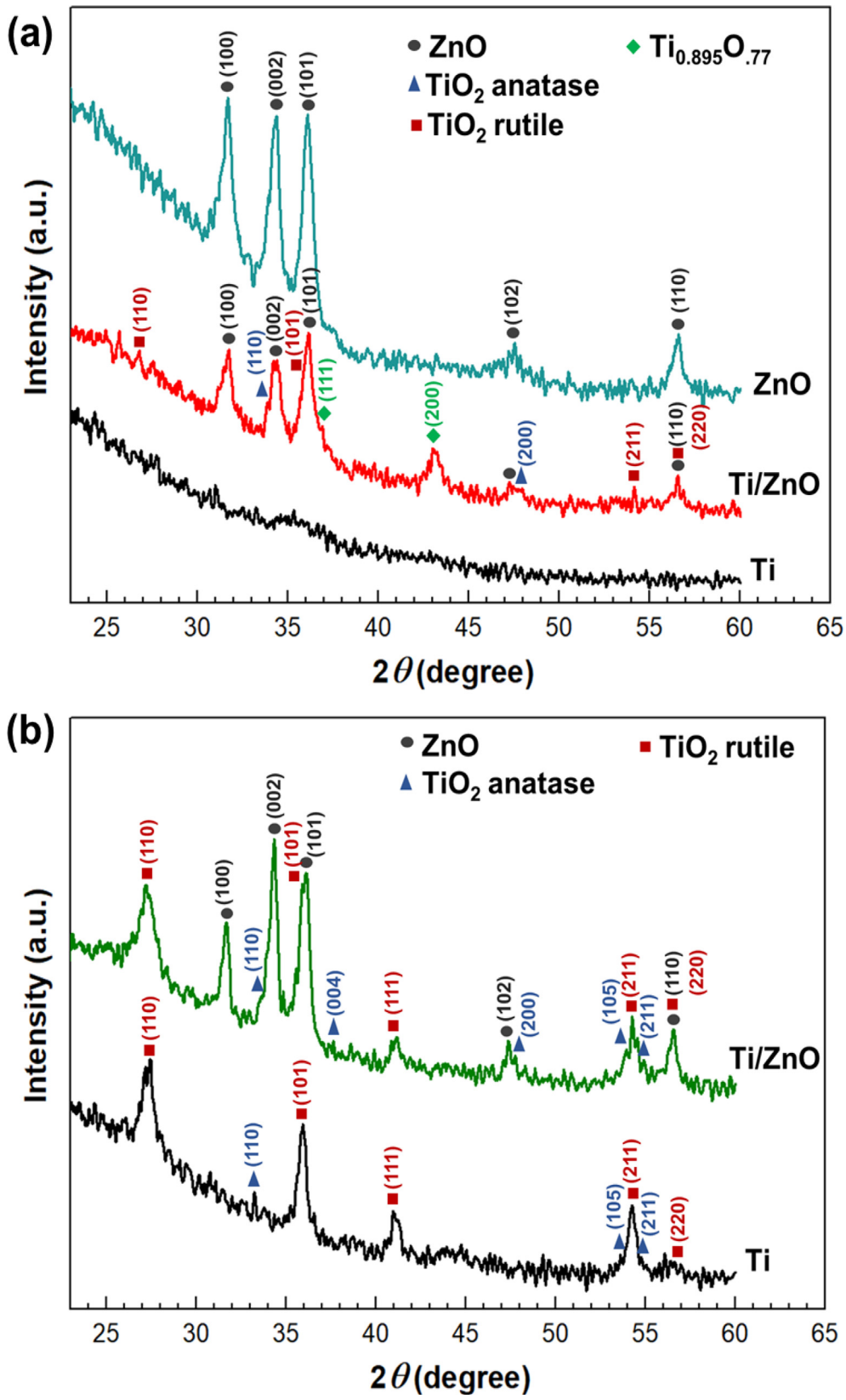

Fig. 2 X-Ray Diffraction (XRD) Pattern of thermally oxidized Zn, Ti and Ti/ZnO thin films at (a) 400 and (b) 500 °C.

sectional field of Ti/ZnO microstructures thermally oxidized at 400 °C. The thin film thickness was observed at around 121.500 and 132.280 nm for ZnO and TiO_2, respectively. Two sections zone (inset A and B) were selected to identify the crystalline phase of thin films' upper and middle areas. The circle area around 90 nm was used to observe the selected

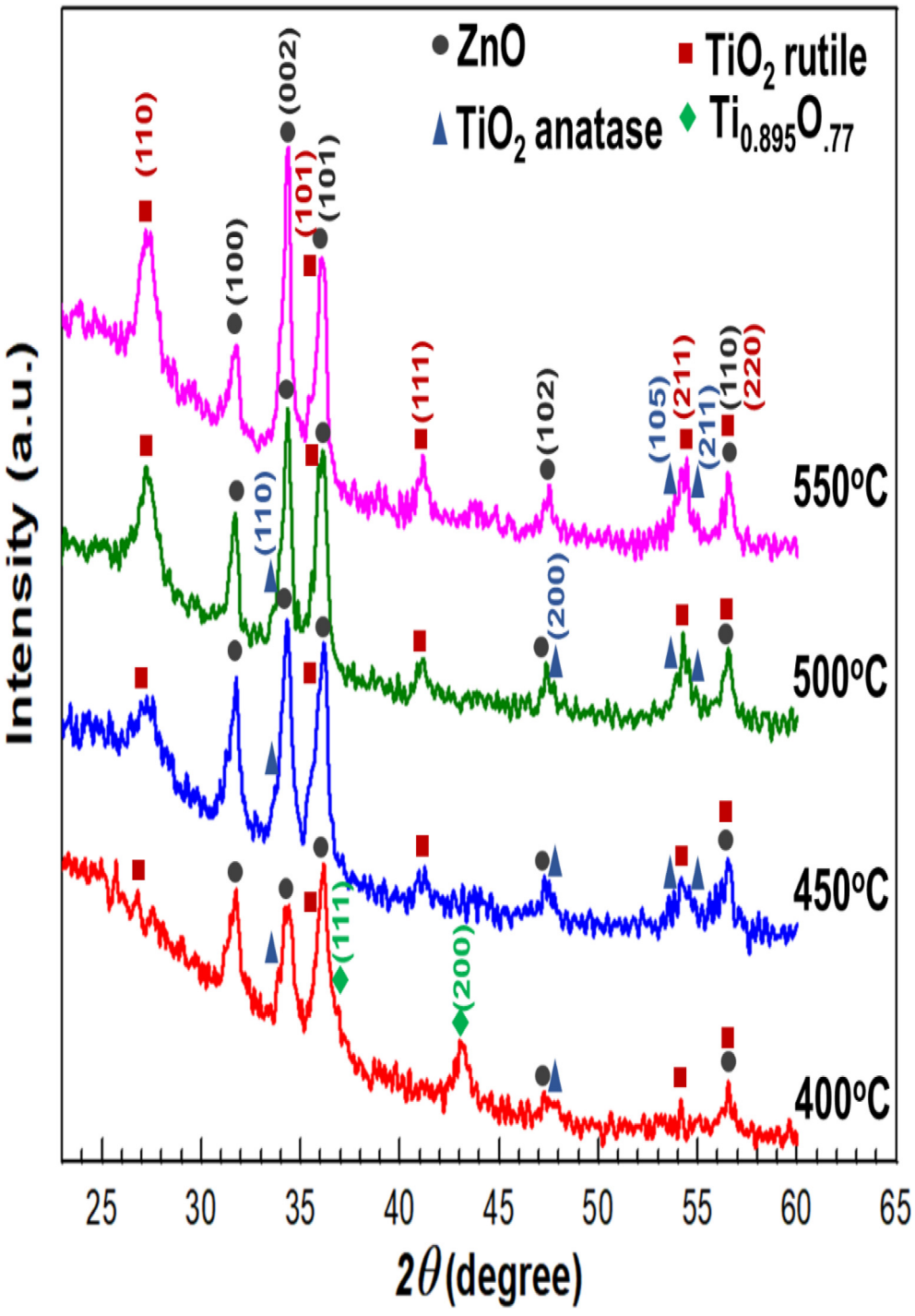

Fig. 3 X-Ray Diffraction (XRD) Pattern of Ti/ZnO bilayer thin films under different oxidation temperatures.

area electron diffraction (SAED). The interplanar distance of 0.351, 0.324, and 0.209 indicated in the image were ascribed to the (1 1 0) anatase, (1 1 0) rutile, and (2 0 0) $Ti_{0.895}O_{.77}$ microcrystalline phase (Fig. 4**b**). Fig. 4**c** displays the SAED pattern of section A, whereas the upper zone area of thin films showed a concentric diffraction ring revealing the polycrystalline of thin films. The (1 1 0) and (1 0 1) anatase, (1 1 0) rutile, and (1 1 1) and (2 0 0) $Ti_{0.895}O_{.77}$ microcrystalline phase were found in this area. Furthermore, in the middle layer of thin films coexisted (1 1 1) and (2 0 0) $Ti_{0.895}O_{.77}$ and (1 0 1) and (2 0 0) ZnO microcrystalline. This observation is consistent with the XRD results, as explained in Fig. 2**a**. $Ti_{0.895}O_{.77}$ phase existed in the middle layer, implying a lack of oxygen content in the film oxidized at 400 °C.

Furthermore**,** Fig. 5 shows HR-TEM micrographs and SAED patterns of Ti/ZnO bilayer thin film sample thermally oxidized at 500 °C. The bright cross-sectional field of the TiO_2/ZnO thin films sample shows a thin film thickness of

Table 2 Optimized lattice parameters of the rutile phase TiO_2 and hexagonal ZnO in TiO_2/ZnO bilayer thin-film samples as a function of oxidation temperature.

Sample	TiO_2				ZnO			
	Crystalline size (*D*) (nm)	Lattice parameter		Unit of Cell volume ($Å^3$)	Crystalline size (*D*) (nm)	Lattice parameter		Unit of Cell volume ($Å^3$)
		$a = b(Å)_{(110)}$	$c\ (Å)_{(101)}$			$a = b(Å)_{(100)}$	$c\ (Å)_{(002)}$	
ICDD		4.593	2.959	62.434		3.250	5.207	54.988
ZnO					18.161	3.251	5.214	55.344
TiO_2	19.993	4.594	2.967	62.609				
Ti/ZnO 400	7.356	4.581	2.959	62.103	17.389	3.257	5.641	59.851
Ti/ZnO 450	8.661	4.614	2.971	63.232	15.746	3.254	5.636	59.675
Ti/ZnO 500	16.251	4.633	2.979	63.936	26.541	3.262	5.650	60.128
Ti/ZnO 550	11.514	4.625	2.976	63.655	24.159	3.266	5.657	60.362

approximately 125.560 and 173.170 nm for ZnO and TiO_2, respectively. This shows that the film has good crystallinity in all zones, as shown in Fig. 5**b to e**. According to HR-TEM and SAED pattern analysis, the crystalline grains belong to the upper layer's thin films' rutile and anatase phases (Fig. 5**b and c**). Instead of anatase and rutile, the ZnO phase also existed on the middle layer, as shown in Fig. 5**d to e**. Literature indicates that TiO_2 growth is triggered in the rutile and anatase mixture phase, and the rutile phase rises with increasing thermal oxidation temperature (Yeh et al., 2018, Lee et al., 2021, Zhou et al., 2013b). During thermal oxidation, increasing oxidation temperature will induce sufficient oxygen to alter Ti layer microstructure and phase development. It must be pointed out that anatase phase still existed at 500 °C, which was due to incorporated of ZnO bottom layer.

3.2. Optical properties and band gap energy

To further determine the optical characteristic of the thin films under various oxidation temperatures, transmission and absorbance were measured using UV–VIS spectroscopy. Transmission spectra as a function of oxidation temperature are displayed in Fig. 6**a**. ZnO, TiO_2, and glass substrates were used as references. The average transmittance in the visible range is around 3.7–78.1 % for TiO_2/ZnO bilayer thin films. Increased visible transmittance is discovered to be a function of oxidation temperature. Enhanced transmittance is responsible primarily for the increased surface area's reaction to light emitted. The optical transmittance spectra of Ti/ZnO thin films thermally oxidized at 400 °C showed only 3.7 % in the visible region. However, oxidation temperature will increase film transmittance to 78.2 % at 500 °C, as seen in Fig. 6.

Enhanced crystallinity of TiO_2 and reduced optical scattering owing to densification of film crystallites, thickness, and defects might contribute to an increase in optical transmittance (Salaken et al., 2013), (Kamaruddin et al., 2011). The lower transmittance in Ti/ZnO bilayer films with 400 °C oxidation temperature could be due to the presence of the (111) and (200) $Ti_{0.895}O_{.77}$, as shown on XRD patterns (Fig. 2**a and** Fig. 3), implying the lack of oxygen content in the film. $Ti_{0.895}O_{.77}$ exhibited higher reflective properties due to inadequate oxygen in films. Ting et al. (Ting et al., 2000) suggested that thin-film transmittance improved by raising the thermal oxidation temperature, which probably removed the residual stress, quantum confinement, and structure order improvement. Similarly, Sreedhar et al. (Sreedhar et al., 2017) demonstrated that transmission in the TiO_2/ZnO composite drops rapidly at about 400 nm, consistent with electron excitation from the valence to the conduction bands. It clearly demonstrates that TiO_2/ZnO films were sensitive to visible light owing to a red shift in the optical absorption edge, which lowered the band gap energy. Furthermore, the transmittance of TiO_2/ZnO bilayer thin films is lower than that of the single layer of ZnO or TiO_2 due to increasing the thickness of the film, leading to a decreasing transmittance.

The optical band gap of TiO_2/ZnO thin films was determined using an indirect band gap semiconductor by plotting the graph of the incident photon energy ($h\nu$) against $(\alpha h\nu)^{0.5}$. The bandgap values in the range of 2.5–3.05 eV of TiO_2/ZnO bilayer film with oxidation temperature are shown in Fig. 6**b**, which is the crucial factor for carrier generation. This is in good agreement with the results reported earlier that showed TiO_2/ZnO films band gap under different TiO_2 thicknesses around 3.18–3.23 eV (Sreedhar et al., 2017). Moreover, the lower value energy band gap was observed in thin-film samples with a lower oxidation temperature. A possible reason is the higher density of donor states near the conduction band, which is governed by the oxygen vacancies on the thin films. This results in good agreement with XRD analysis that shows Ti/ZnO thin films thermally oxidized at 400 °C have a $Ti_{0.895}O_{.77}$ phase that implies a lack of oxygen content in the film.

TiO_2 shows an indirect bandgap while ZnO displays a direct bandgap, with corresponding E_g values of 3.14 eV and 3.26, respectively. The combination of ZnO and TiO_2 material reduced the energy band gap and could improve the minimum energy required for excitation electron. The electron will become quickly excited from the valence band to the conduction band (Firdaus et al., 2012). Hernandez et al. (Hernández et al., 2014) similarly observed band gap reduction of TiO_2/ZnO samples due to several possibilities, such as (i) functional band gap distinction among anatase TiO_2 (3.2 eV) and ZnO (3.37 eV), (ii) rising of TiO_2 content on the ZnO surface (Yan et al., 2012), (iii) interlayer Fermi level equalization arrangement (Kalanur et al., 2017) and (iv) The Burstein-Moss (BM) effect (Pérez-González et al., 2017).

This finding showed that the transmittance and energy band gap increased as a function of oxidation temperature. It is known that the thermal oxidation process of TiO_2/ZnO bilayer thin film is a controlled mechanism of oxygen diffusion.

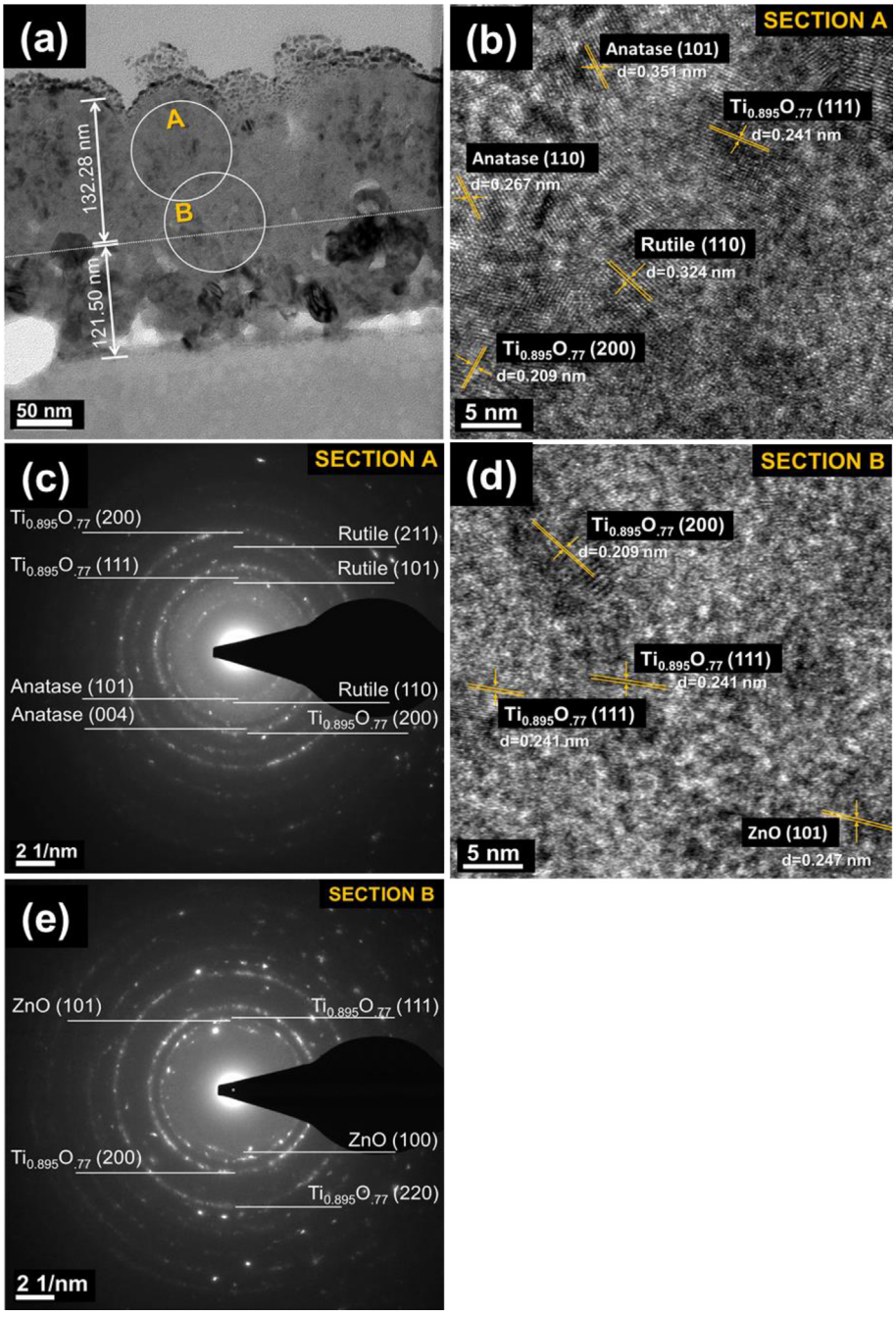

Fig. 4 Cross-sectional Transmission Electron Microscopes (TEM) images of a thermally oxidized Ti/ZnO thin film sample at 400 °C: (a) bright field of the film with a thickness of 253.78 nm. The images (inset A and B) were selected for High-Resolution TEM and electron diffraction analysis: (b) HR-TEM image showing point "A" (c) Selected area diffraction (SAED) pattern of section "A" adjacent to anatase, rutile and $Ti_{0.895}O_{.77}$, (d) HR-TEM image showing point B, and (e) SAED pattern of section "B" adjacent to $Ti_{0.895}O_{.77}$ and ZnO.

Increasing thermal oxidation temperature could be attributed to the reduction of oxygen vacancies in the films, which increases transmittance and energy band gap. Consequently, Alteration in oxidation temperature is emphasized here as a viable method for transmittance and band gap adjustment and collecting a greater proportion of incoming light. In addition, the increased film crystallinity is linked to a shift in the optical absorption edge towards the visible light range, improving charge carrier mobility concerning recombination rate.

3.3. Photocatalytic activity

The photocatalytic activity of thin-film samples was investigated by decomposition of MB solution under UVA irradiation. All thin films sample display increasing photocatalytic activity as a function of irradiation time, as shown in Fig. 7**a**. The MB degradation percentage for Ti/ZnO sample thermal oxidized at 400, 450, 500 and 550 °C were 54.641, 69.128, 85.021 and 87.009 %, respectively. It showed that the degradation efficiency of the Ti/ZnO thin films increases by

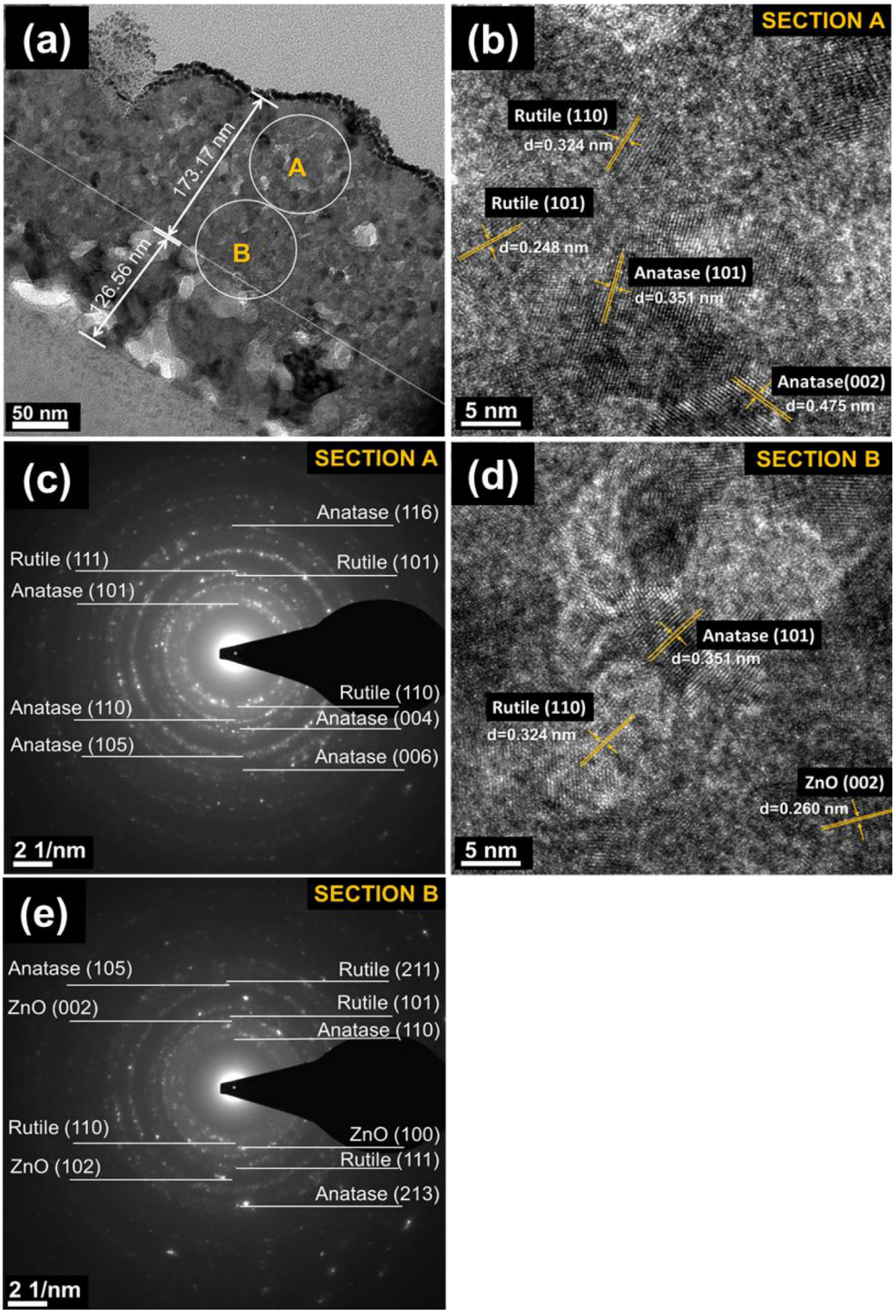

Fig. 5 Cross-sectional Transmission Electron Microscopes (TEM) images of a thermally oxidized Ti/ZnO thin film sample thermally oxidized at 500 °C: (a) bright field of the film with a thickness of 299.73 nm. The images (inset A and B) were selected for High-Resolution TEM and electron diffraction analysis: (b) HR-TEM image showing point "A" (c) Selected area diffraction (SAED) pattern of section "A" adjacent to anatase and rutile (d) HR-TEM image showing point B, and (e) SAED pattern of section "B" adjacent to anatase, rutile and ZnO.

increasing oxidation temperature. The highest degradation efficiency was found for Ti/ZnO thermal oxidized at 550 °C. The pure TiO_2 thin films sample shows only 53.510% of MB degradation percentage. TiO_2/ZnO thin films exhibit significantly higher photocatalytic performance than TiO_2 thin films. However, the degradation efficiency of ZnO single layer and TiO_2/ZnO bilayer are comparable, around 88.601 and 87.009%, which were the highest among the samples.

The possible reason is that ZnO is the primary source of photogenerated charge carriers, and its surface reactions

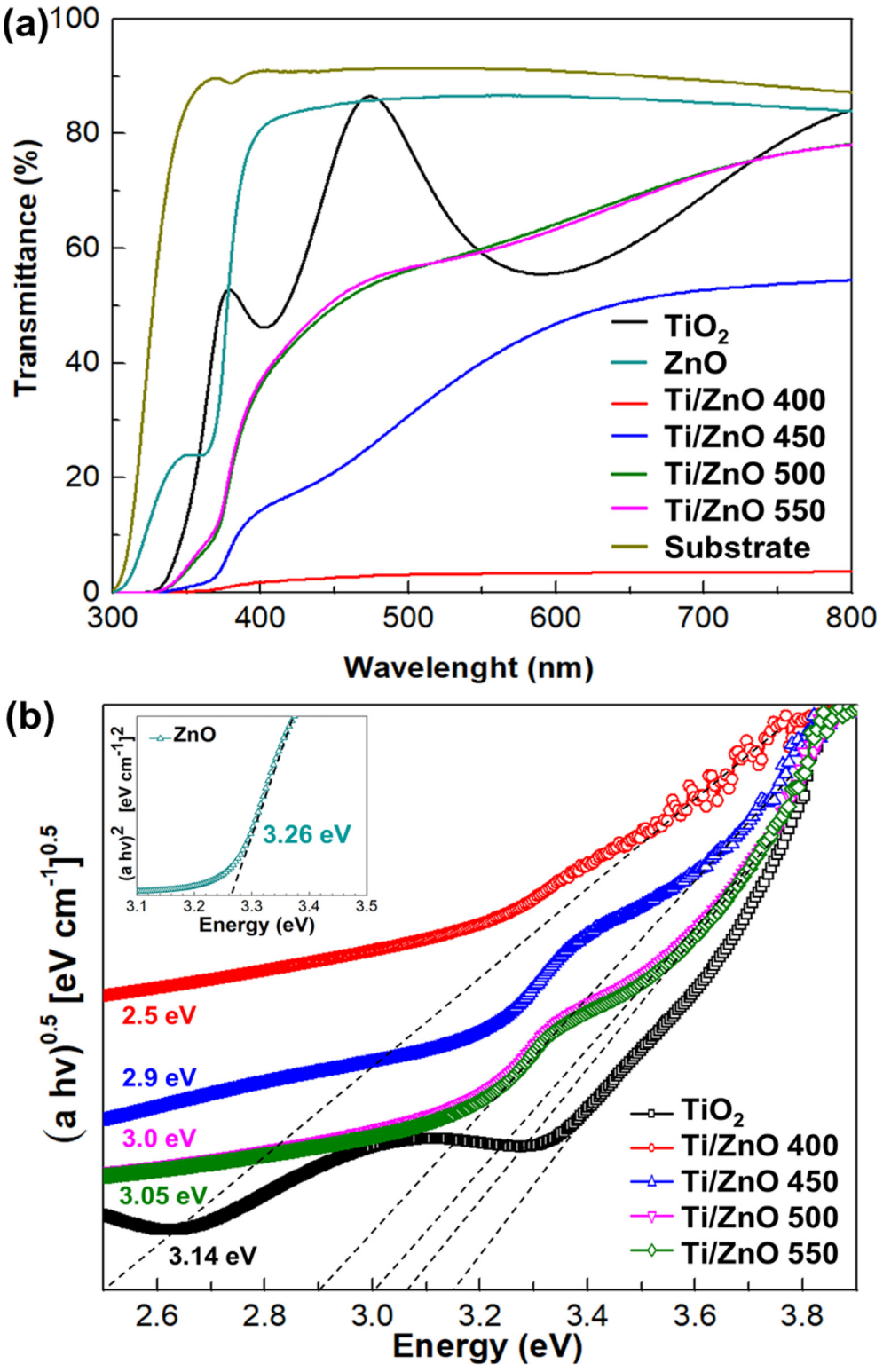

Fig. 6 Optical properties of TiO_2/ZnO thin films. **(a)** Transmittance of the TiO_2/ZnO thin films under various oxidation temperatures. **(b)** Plot of $(\alpha hv)^{0.5}$ versus photon energy (hv) of the TiO_2/ ZnO thin films under different oxidation temperature (**inset**: plot of $(\alpha hv)^2$ versus photon energy (hv) of the ZnO thin films).

proceed unobstructed. The inclusion of TiO_2 thin films on the ZnO layer could limit the wavelength of light absorbed due to the shift in the absorption edge to shorter wavelengths (Butalid et al., 2020). This phenomenon causes slightly lower degradation efficiencies when compared to ZnO single layer.

The kinetics of MB photodegradation on the thin film surface can be described by the Langmuir-Hinshelwood (LH) first-order reaction kinetics Equation (**Eq. (4)**): (Lee et al., 2021)

$$\ln \frac{C_t}{C_0} = -kt \tag{4}$$

As illustrated in Fig. 7**b**, the ln (C_t/C_0) is the linear fit slope in the function of the time (t) plot shows the kinetic constant (k) of the photodegradation. The photocatalytic reaction process was matched with the pseudo-first-order reaction kinetics. The reaction constants (k) of the ZnO, TiO_2 and Ti/ZnO thin films oxidized at various temperatures are listed in Table 3.

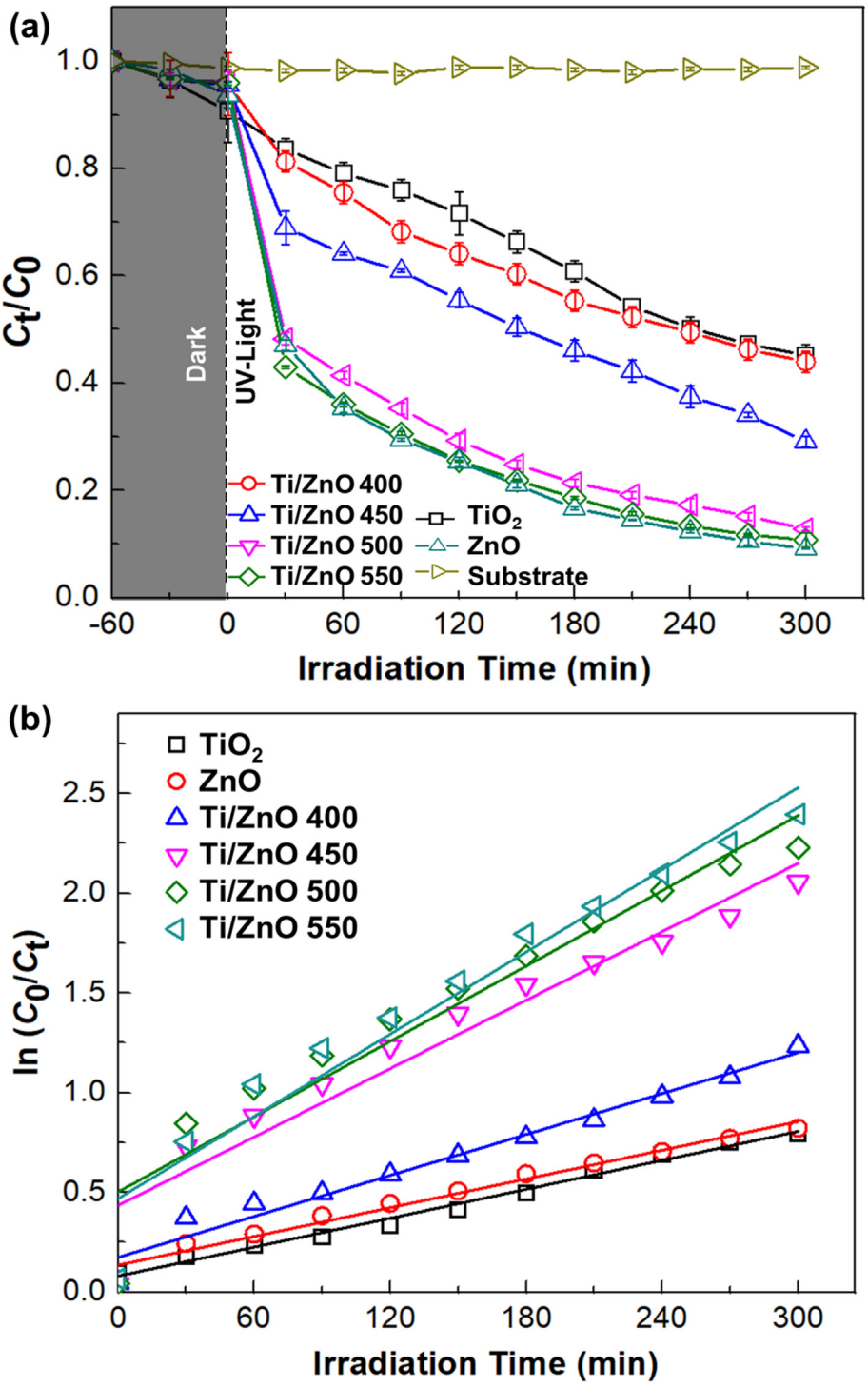

Fig. 7 Photodegradation of Methylene Blue (MB) solution by photocatalytic reaction with TiO_2/ ZnO thin film under UV-light (λ = 365 nm) irradiation and (b) Kinetics curves (first-order reaction) of thin films samples with MB under various oxidation temperature. The experimental condition is: MB concentration (C_0) = 10 mg/L, T = 25 ± 2 °C.

Linear fits are in good agreement ($R^2 > 0.90$) with the LH model. The degradation rate constant (k) gradually increases with an increased oxidation temperature. However, a decrease in the photocatalytic activity and rate constant (k) was observed on Ti/ZnO thin films that oxidized at 400 °C. The decrease could be attributed to the existence of the (1 1 1) (2 0 0) $Ti_{0.895}O_{.77}$ phase, which also decreases the optical transmittance, as shown on XRD analysis **(**Fig. 2**a).** In the thin-film crystal structure, defect states (such as oxygen vacancies) are well-known to cause decreased photocatalytic activity.

A slight decrease in the rate constant was observed when TiO_2 was applied to the ZnO surface. The reduction may be ascribed to the blueshift of the TiO_2-coated ZnO film's absorption edge related to that of ZnO film (Butalid et al., 2020). It is known that the crystal structure influences photocatalytic efficiency. TiO_2 photocatalytic activity may be improved on its (1 0 1) and (0 0 1) faces, while ZnO is optimized on its zinc-terminated polar (0001) (Zhou et al., 2019). In addition, the band gap's energy is crucial to the thin film photocatalytic capabilities.

Semiconducting photocatalysts are highly dependent on the dissociation of the photogenerated hole–electron pairs and the transport of electrons from the photocatalyst into organic pollutants trapped inside oxygen vacancy defects on the surface (Yu et al., 2020). Yi Zhou et al. (Zhou et al., 2019) reported that the higher band conduction band (*cb*) of TiO_2 allowed charge transfer from ZnO to TiO_2 through a direct Z-scheme photocatalytic mechanism. A possible photocatalytic reaction process for TiO_2/ZnO bilayer thin film has been proposed in Fig. 8. TiO_2/ZnO is a heterogeneous semiconductor-based photocatalysis approach with a bandgap of around 3.2–3.34 eV (Hernández et al., 2014; Tekin et al., 2020). In the presence of UVA light, electrons will migrate from *vb* (h^+_{vb}) to *cb* (e^-_{cb}) **(Eqs. (5) and (6))** due to higher energy photons than in the thin film bandgap. Photogenerated electrons (e^-_{cb}andh^+_{vb}) rapidly react with the adsorbed oxygen and water molecule to produce highly reactive hydroxyl radicals (·OH) **(Eq. (8))** and superoxide anions radical ($O_2^{\cdot-}$) **(Eq. (7))** (Vinu and Madras, 2010). Accordingly, it can be inferred that the heterojunction defect levels do not significantly alter photocatalytic activity. In addition, the electron-hole pairs are separated because the electrons remain in the *cb* of TiO_2, where the hole remains in the *vb* of ZnO, which reduces the recombination rate and enhances the photocatalytic activity of TiO_2/ZnO bilayer thin films. The following equations describe how photocatalytic reaction of TiO_2/ZnO thin films (**Eqs. (5)–(12)**):

$$ZnO + h\nu \rightarrow ZnO + e^-_{cb} + h^+_{vb} \quad (5)$$

Table 3 Dependence of rate constant (k) values against oxidation temperature in TiO_2/ZnO bilayer thin film.

Sample	*Rate constant* (k)x10^{-3}, min^{-1}	Correlation coefficient (R^2)
ZnO	6.860	0.988
TiO_2	2.410	0.974
Ti/ZnO 400	2.400	0.969
Ti/ZnO 450	3.420	0.923
Ti/ZnO 500	5.710	0.916
Ti/ZnO 550	6.290	0.942

$$TiO_2 + h\nu \rightarrow TiO_2 + e^-_{cb} + h^+_{vb} \quad (6)$$

$$e^-_{cb} + O_2 \rightarrow O_2^{\cdot-} \quad (7)$$

$$h^+_{vb} + H_2O \rightarrow {}^{\cdot}OH + H^+ \quad (8)$$

$$O_2^{\cdot-} + H^+ \rightarrow HO_2^{\cdot} \quad (9)$$

$$O_2^{\cdot-} + 2H_2O \rightarrow 3\,{}^{\cdot}OH + {}^{-}OH \quad (10)$$

$$O_2^{\cdot-} + HO_2^{\cdot} + H^+ \rightarrow H_2O_2 + O_2 \quad (11)$$

$$H_2O_2 + e^- + \cdot OH \rightarrow \cdot OH + {}^{-}OH \quad (12)$$

This study revealed that the photocatalytic of TiO_2/ZnO thin films depends on the oxidation temperature that affects the crystalline phase. It could be noted that the addition of ZnO as bottom layer thin films could promote increasing photocatalytic activity of TiO_2 thin films. These studies indicate that the oxidation temperature is crucial in obtaining the high photocatalytic performance of TiO_2/ZnO bilayer thin films.

A number of studies have demonstrated the photocatalytic activity of ZnO-TiO_2 thin films prepared with various methods, as listed in Table 4. However, the photocatalytic activity of TiO_2/ZnO bilayer thin films produced by magnetron sputtering combined with thermal oxidation techniques has been described in only a few published studies. At the same irradiation time, the photocatalytic activity obtained in this research is higher than TiO_2/ZnO developed with the sol–gel method (Hussin et al., 2019), (Pérez-González et al., 2015) and reactive magnetron sputtering (MS) (Pérez-González et al., 2017). However, this study's photocatalytic results were lower than Butalid et al. [37]. Several factors influence the photocatalytic activity of thin films, such as thin-film profile (thickness, morphology, element composition, crystallinity, band gap energy, etc.), the pollutant type and concentration, and irradiation condition (type, light intensity, time). This research revealed that the development of TiO_2/ZnO thin films by thermal oxidation could enhance the high photocatalytic activity of thin films.

Catalyst reusability is an important aspect of thin film catalysis. Five consecutive cycle tests were applied to show further the photostability of thin-film samples on the removal of MB solution. Fig. 9 showcases thin films' degradation rate stability profile under 300 min UV irradiation time. It can be observed that different thin films sample showed different MB degradation profiles. Among them, ZnO thin films demonstrated the weakest photostability, which promotes decrease of 25.952 and 57.698% degradation efficiency after three and five cycles, respectively, as shown in Fig. 9**a.** However, there were less significant changes in the degradation efficiency of the TiO_2 (6.570%) (Fig. 9**b**) and TiO_2/ZnO (4.029%) (Fig. 9**c**) bilayer thin film samples in five consecutive cycle tests. A comparison of the XRD patterns of the initial and 5 times reused TiO_2 and ZnO thin films is shown in **Supplementary material B, Fig. B1. Fig. B1a (Supplementary material B)** indicates that there were no additional phases, and this result is almost similar to the initial TiO_2 thin film. However, in ZnO thin films show there are decreasing peak intensity after 5 times used (**Supplementary material B, Fig. B1b**). This finding demonstrates that TiO_2 films are photochemically stable even after being reused 5 times, since the crystalline structure of the films

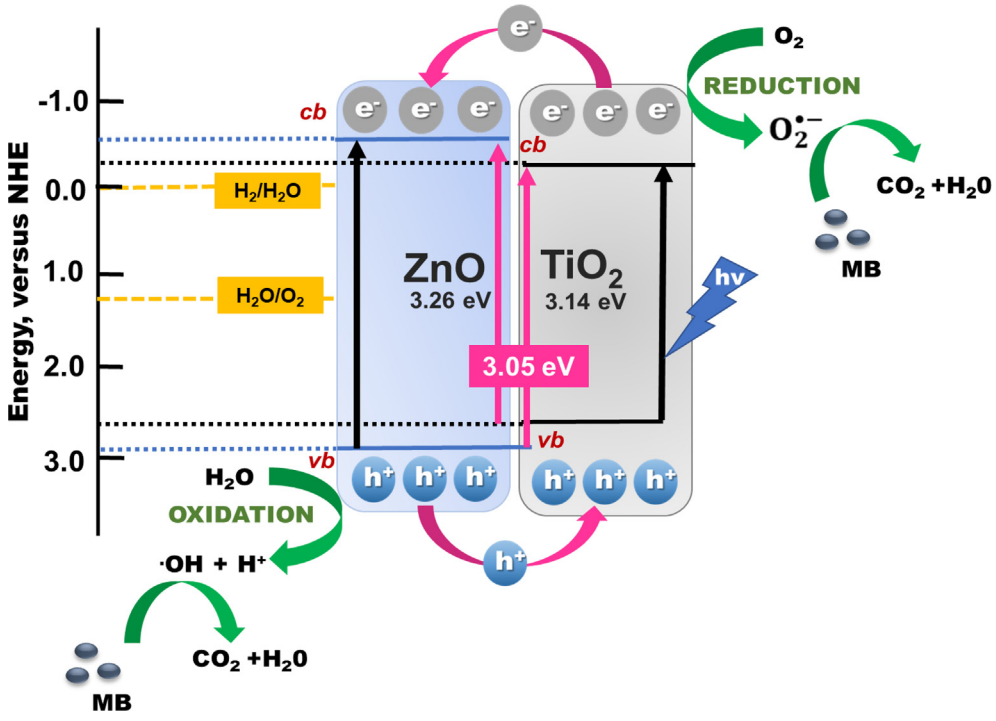

Fig. 8 Proposed photocatalyst schematic diagram of the TiO_2/ZnO bilayer thin film.

Table 4 Photocatalytic activity of TiO_2/ZnO thin films prepared with various method.

Fabrication	Thickness (nm)	Irradiation condition, time	Pollutant and Concentration	Photocatalytic activity (%)	Refs.
Sol-gel	80	UVC lamp (15 W), 120 min	MB (10 mg/L)	59	(Pérez-González et al., 2015)
Reactive MS	73	UVC lamp (15 W), 120 min	MB (10 mg/L)	44	(Pérez-González et al., 2017)
Sol-gel (bilayer)	–	UV lamp, 300 min	MB (10 mg/L)	43.5*	(Hussin et al., 2019)
Reactive MS (bilayer)	620	UVB lamp (25 W), 150 min	MO (10 mg/L)	78	(Ton et al., 2020)
Reactive MS (bilayer)	147	Xenon lamp (1000 W), 180 min	MB (10 mg/L)	94.3	(Butalid et al., 2020)
MS, thermal oxidation (bilayer)	298	UVA (8 W) 120 min 150 min 240 min 300 min	MB (10 mg/L)	72.644 76.160 84.459 87.099	**This Work**

*Calculated from At/Ao.
MO (Methyl Orange); MB (Methylene Blue); MS (Magnetron Sputtering).

remains the same despite subsequent degradations, with the intensity of the peak only slightly increasing.

This finding indicates that the addition of TiO_2 as the upper layer on ZnO thin films was seen to decrease the photo corrosion of ZnO during photodegradation. Removing photocatalytic material by photo corrosion would decrease the photocatalytic efficiency due to a reduction in generated charge carriers. Butalid et al. (Butalid et al., 2020) have reported that Zn^{2+} was obtained in the MB solution, which had a high concentration on ZnO thin films that TiO_2/ZnO thin films after the third cycle of photodegradation of ZnO thin film. Furthermore, Ikizler and Peker (İkizler and Peker, 2016) investigated the spin coated TiO_2 on hydrothermally grown ZnO nanorods. These results showed that the concentration of Zn^{2+} ions decreased from 1.1 to 0.6 ppm when ZnO surfaces were coated with TiO_2. However, lower Zn^{2+} ions were still found on the samples due to the incompleteness of the TiO_2 coating, resulting in areas on the ZnO surface with pitting corrosion; hence the observed. This is attributed to the effect of photo corrosion that caused the dissolution of the ZnO thin films. Photo corrosion issue as a ZnO drawback could reduce the degradation efficiency and shorten the cata-

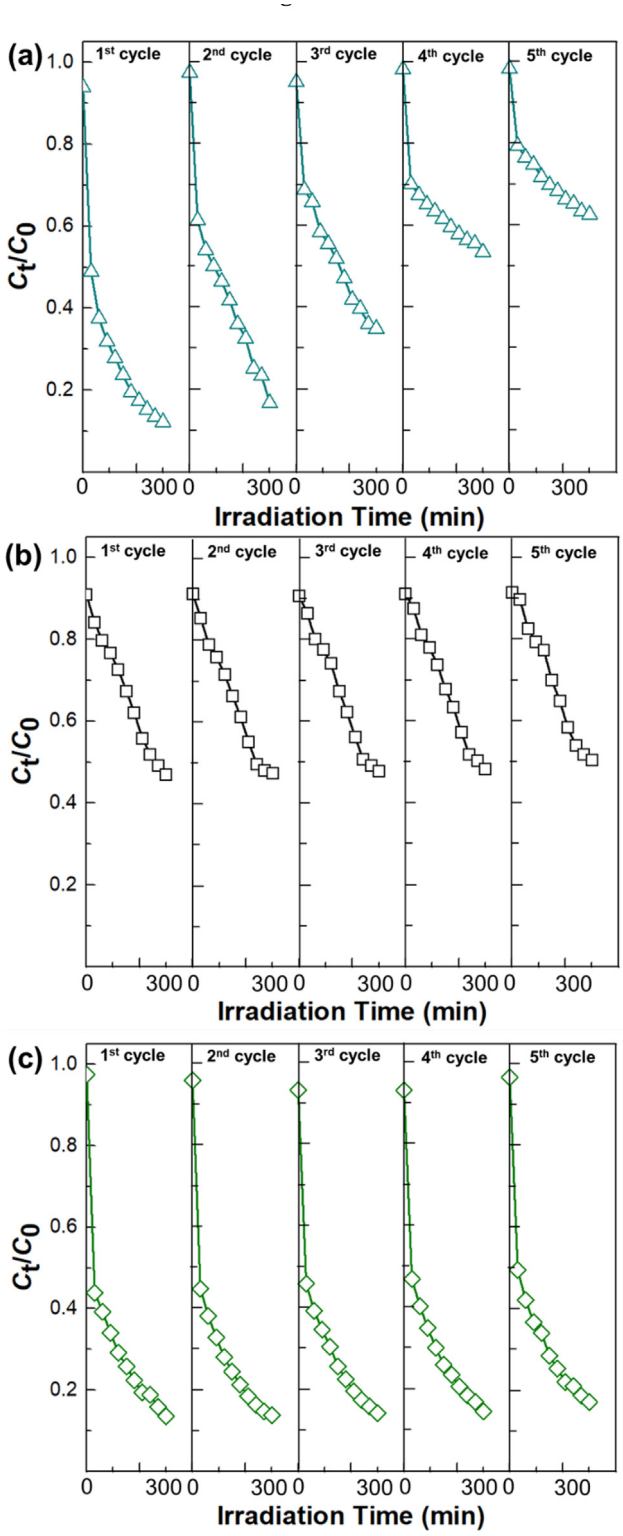

Fig. 9 Photocatalytic stability performance of (a) ZnO and (b) TiO_2 and (c) TiO_2/ZnO bilayer toward photodegradation of Methylene Blue solution under 300 min of UV irradiation.

lyst lifetime. furthermore, Zn^{2+} ions may also harm waterborne microbes if the concentration is above a certain threshold (Franklin et al., 2007), (İkizler and Peker, 2016). This result confirms that protective layers such as TiO_2 minimize the effect of photo corrosion which promotes high recyclability and photocatalytic activity of TiO_2/ZnO thin films. Further analysis was established to investigate the correlation between the photocatalytic activity and antimicrobial activity of ZnO, TiO_2 single layer, and TiO_2/ZnO (thermal oxidized 550 °C) bilayer thin films.

3.4. Antimicrobial activity

The antimicrobial behavior of synthesized thin-film samples against gram-negative (*E. coli*), positive bacteria (*S. aureus*), and pathogenic yeast (*C. albicans*) was evaluated using an agar diffusion test. The diameter of clear zones, which indicates inhibition of microbe growth, was used to determine the antimicrobial activity. The antimicrobial behavior was evaluated in the absence of light (dark), visible and UVA light with a 30-minute exposure time, as displayed in **Supplementary material C, Fig. C1**. In the dark condition, no inhibition zone is found in all samples. However, introducing a visible light condition for TiO_2/ZnO and TiO_2 thin film samples could somewhat inhibit the growth of *E. coli* and *S. aureus*. In addition, the inhibition zones have started to increase under UVA light exposures with a diameter zone of around 33.7, 28.13, and 33.23 mm for ZnO, TiO_2, and TiO_2/ZnO thin films, respectively (**Supplementary material C, Table C1**). These inhibition diameters are nearly equal to or even more extensive than the diameter of the antibiotic used as a positive control. Previous studies investigated the zone inhibition analysis of TiO_2/ZnO nanocomposite using different bacteria such as *E.-coli* (19.7 mm) (Ali et al., 2021), (25 mm) (Vignesh et al., 2017), and *S. aureus* (21.38 mm) (Harun et al., 2018), (17.67 mm) (Siwińska-Stefańska et al., 2019) (**Supplementary material C, Table C2**). which showed relevance to the present study. The light has a significant advantage when comparing the antimicrobial activity of dark, light, and UVA inhibition zones. The results proved that assimilation of the photocatalyst with UVA light conditions significantly influenced antimicrobial behavior compared to visible light or dark conditions. Further analysis was established to examine the effectiveness time of UVA light exposure on thin films against three types of microbes.

Fig. 10 presents exposures of ZnO, TiO_2, and TiO_2/ZnO thin films under 10 min UVA irradiation could exhibit a significant inhibition rate (%) ($p < 0.05$) against three types of microbes with an average inhibition rate of 58.222, 44.444 and 77.111 %, respectively. The negative controls showed a low inhibitory effect (< 5%), and antibiotics as positive controls showed a 94% inhibition rate. It could be seen that the TiO_2/ZnO inhibition rate at 10- and 20-min irradiation is significantly higher than in ZnO and TiO_2 thin films. However, after a 30-min irradiation time, the inhibition rate was not significantly different for ZnO and TiO_2/ZnO films. Under different irradiation times, TiO_2 exhibits less antimicrobial activity than ZnO and TiO_2/ZnO thin films. Furthermore, increasing the UVA exposure time to 30 min results in a high inhibition rate of 97.733 ± 3.05, 98.07 ± 2.41, and 95.800 ± 3.11% against *E. coli*, *S. aureus*, and *C. albicans*, respectively (Fig. 10). These inhibition rates are close to those of antibiotics as a positive control. Increased irradiation exposure time resulted in a substantial enhancement in the inhibition rate against the three pathogenic microbes. Although integrating

photocatalyst with UVA light to decrease microbial growth is not new, this present study confirmed that exposure time responses of antimicrobial activity to increased inhibition values demonstrated the time-sensitive properties of UVA irradiation as a potential and fast disinfection.

The antimicrobial effect on ZnO, TiO_2, and TiO_2/ZnO thin films against three types of pathogenic microbes could be due to several mechanisms, as illustrated in Fig. 11. First, the electrostatic interaction between the positive charge of TiO_2/ZnO and the negative charge of the microbe cell might result in instability of the microbial cell wall. The instability of the microbial cell wall could cause membrane disruption, morphological changes, and intracellular substance liberation (Brayner et al., 2006). Moreover, the release of Zn^{2+} ions from ZnO thin films under UV light irradiation (Butalid et al., 2020; Sapkal et al., 2012; Vignesh et al., 2017) has the potential to damage the integrity of microbial cells that serve as a crucial cellular defense mechanism for regulating zinc excess and deficiency (Kasemets et al., 2009) (Joe et al., 2017). It is noted that increasing irradiation time could increase Zn^{2+} ion concentration, which promotes high antimicrobial activity. However, applying TiO_2 as the upper layer on ZnO (TiO_2/ZnO) reduced the photocorrosion effect (Butalid et al., 2020), (Sapkal et al., 2012) and resulted in a decrease in Zn^{2+} ion concentration that could only cause minor antimicrobial activity.

During the photocatalytic process, the reactive hydroxyl radical (•OH), superoxide anions radical (O_2^-), and hydrogen peroxide (H_2O_2), known as Reactive Oxygen Species (ROS), cause serious damage to microorganisms (Abebe et al., 2020; Espitia et al., 2012; Gordon et al., 2011). ROS promotes the oxidation of cellular structures that promote partial loss of cell membrane integrity, permeabilization of cell membrane, exposed cellular component. As a results, leads to the complete microbial inactivation (**Equation (13)**) (Afreen et al., 2020; Yemmireddy and Hung, 2017).

$$\text{Microorganism} + [{}^{\cdot}OH; O_2^{\cdot-}; HO_2^{\cdot}; {}^{-}OH] \rightarrow \text{membrane cell disrupt} \rightarrow \text{exposed cellular component} \rightarrow \text{microbial inactivation} \quad (13)$$

Srinivinas et al. (Srinivas et al., 2019) have shown that ROS-induced stress may disrupt microbe structure, leading to a lack of selective function and energy (ATP) synthesis, which impacts DNA replication.

The significant **antimicrobial** activity enhancement of TiO_2/ZnO thin films can be ascribed to the UV irradiation and the thin film properties (crystallinity and crystalline size). As mentioned in Table 2, TiO_2/ZnO thin films have a smaller crystalline size and a larger unit cell volume than ZnO and TiO_2; thus, this condition may promote a high number of photocatalytic reactions sites. The increased photocatalytic reaction sites forge a more considerable amount of ROS that enhances antimicrobial performance. In addition, oxidation of Ti/ZnO at 550 °C could promote the high crystal structure of ZnO wurtzite, anatase, and rutile TiO_2. Instead of the high antimicrobial activity of ZnO, the mixed phase of TiO_2 rutile and anatase can also promote higher photocatalytic activity than a single TiO_2 phase. The electrons from the rutile to anatase TiO_2 during photoexcitation may avoid charge recombination in the rutile phase (Kalarivalappil et al., 2019; Zhu et al., 2018), producing efficient photogenerated electron-hole pair

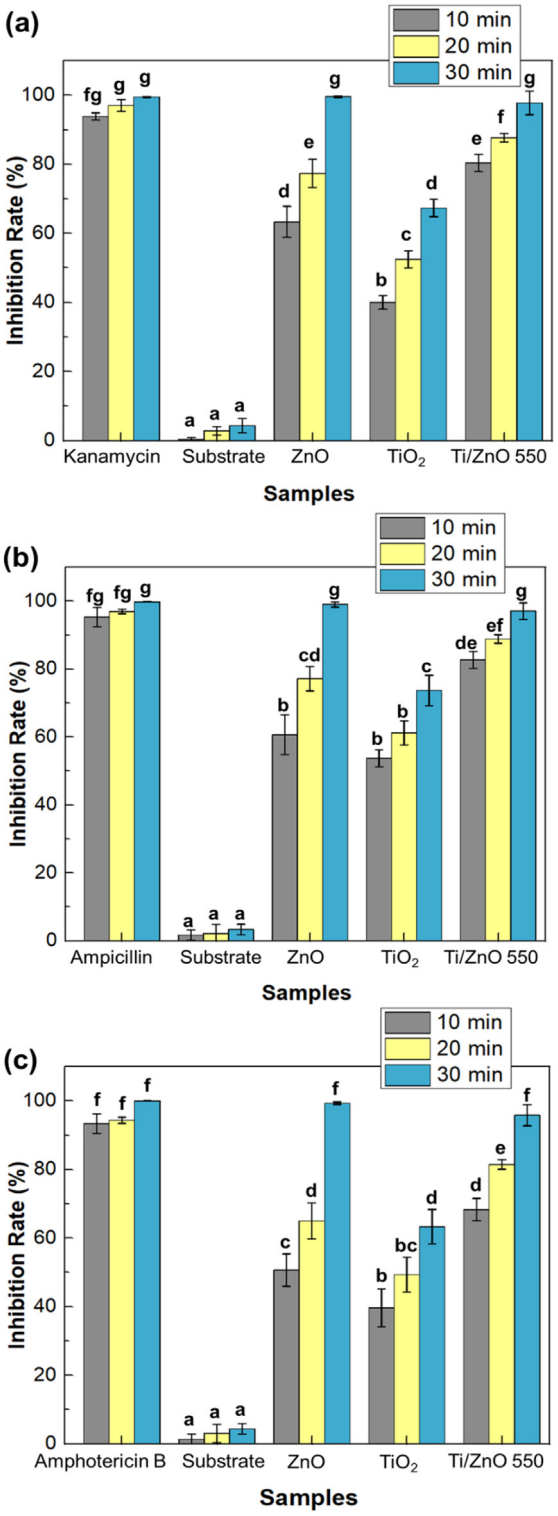

Fig. 10 Effect of ZnO, TiO_2 and TiO_2/ZnO thin films on antimicrobial activity against *E. coli, S. aureus* and *C. albicans* compared to the substrate (negative control) and antibiotic (positive control) under different UV light irradiation treatments. Means denoted by a different letter indicate significant differences between treatments ($p < 0.05$; Tukey HSD test). The data was expressed as mean ± standard deviation ($n = 3$).

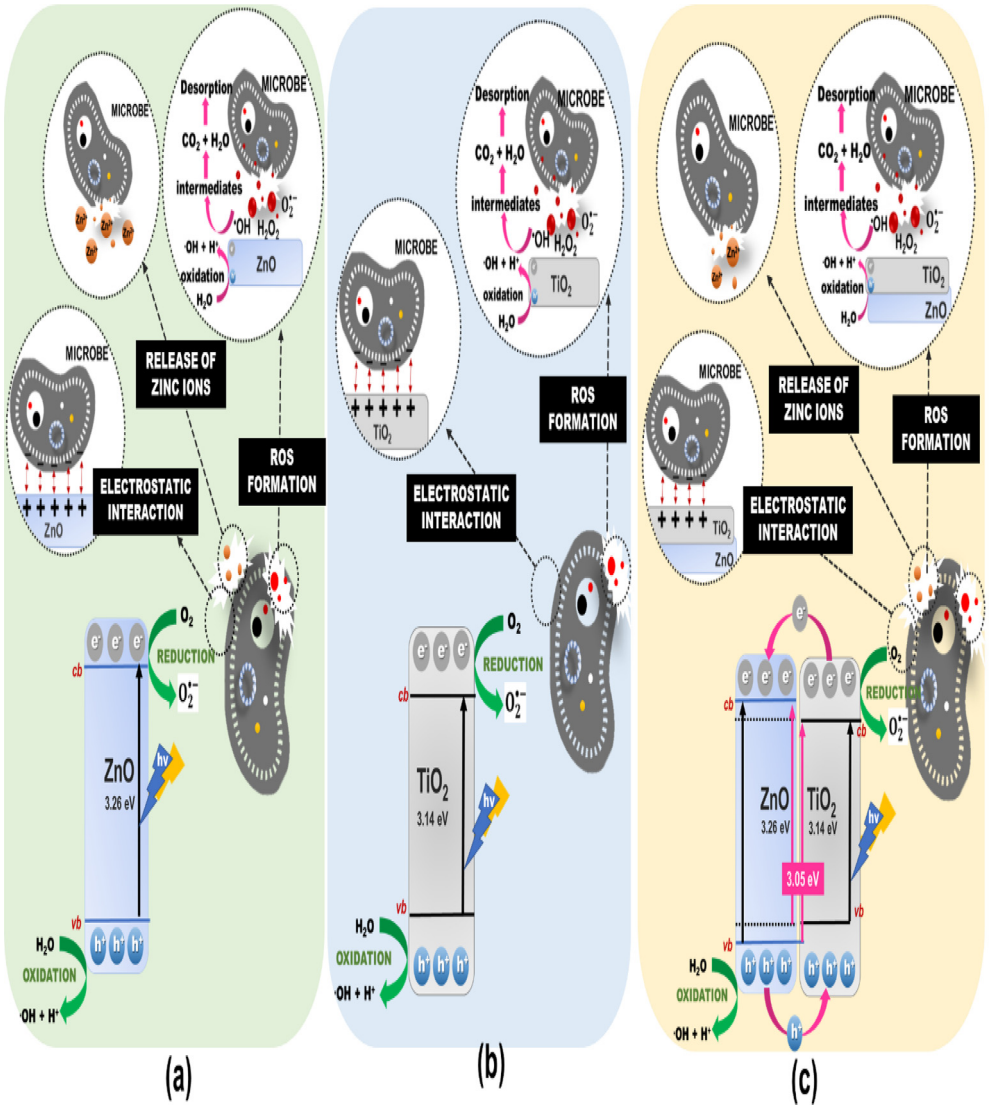

Fig. 11 Proposed antimicrobial based photocatalytic mechanism of (a) ZnO, (b) TiO_2, and (c) TiO_2/ZnO thin films.

separation and high photocatalytic and high antimicrobial performance. Furthermore, adding a TiO_2 layer could reduce rapid recombination on ZnO thin films, enhancing the efficient photocatalytic and antimicrobial activity of TiO_2/ZnO thin films. Antimicrobial inhibition and photocatalytic activity were found to have a strong linear relationship in the thin film sample. The antimicrobial activity of the thin film sample is related to various characteristics, including surface chemistry and microbe concentration, as well as the intensity of the light (Adams et al., 2006).

The photographs of the viable microbe colonies (white spots) on the different irradiation times of TiO_2/ZnO thin films are shown in Fig. 12. The viable microbe colony shows that TiO_2/ZnO thin film could inhibit bacterial growth, whereas increasing irradiation exposure time resulted in a decreased viable microbe colony. In particular, *S. aureus* showed considerably greater sensitivity (98.07%) to TiO_2/ZnO thin films than *E. coli* (97.73%) and *C. albicans* (95.8%) under 30 min irradiation. Similar to the study reported by Widyastuti et al. (Widyastuti et al., 2021) and Russell (Russell, 2003), which mentioned that *E. coli* is more resistant to ROS than *S. aureus*. Structural changes in the bacterial cell membrane significantly contribute to increased resistance. *E. coli* has an exterior cell membrane made mostly of lipopolysaccharide (LPS) and a very thin peptidoglycan layer (Epand and Epand, 2009), which serves as a barrier to block the entry of reactive oxygen species (ROS) into the cell. Moreover, this structure is more complex than *S. aureus* (Russell, 2003). Furthermore, Fig. 12 indicates that the antibacterial activity (*E. coli and S. aureus*) of TiO_2/ZnO seems stronger than antifungal activity (*C. albicans*). Then, it is widely known that fungi have a greater tolerance to the adverse external environment than bacteria due to their thicker cell walls and spore generation capacity (Asare et al., 2022; Probst et al., 2022).

Numerous researchers have assessed the antibacterial activity of TiO_2/ZnO in various morphologies, as listed in Table 5. However, there has been limited research on the antimicrobial activity of TiO_2/ZnO thin films. The antimicrobial activity of TiO_2/ZnO thin films that were developed in this work showed higher inhibition activity with a fast disinfection time than

those reported formerly. Meanwhile, using UVA light as an irradiation lamp during photocatalyst contact time is promising to encourage fast and high antimicrobial activity.

These findings suggest that the thermal oxidation temperature of Ti/ZnO bilayer thin films plays a crucial role in generating good photocatalytic and antimicrobial performance. Moreover, Ti/ZnO thin film through 550 °C thermal oxidation could provide ZnO wurtzite, anatase, and rutile TiO_2 crystal phases with good photocatalytic activity and higher antimicrobial activity. This study reveals that incorporating the magnetron sputtering with the thermal oxidation method may enhance the efficacy of TiO_2/ZnO bilayer thin films as photocatalysts and antimicrobial agents toward pathogenic bacteria and fungus. Therefore, the synthesized TiO_2/ZnO thin films embodied with UV irradiation lamps appear to be a promising antimicrobial coating with good opportunity for industrial scaling up and being a cost-effective and time-effective material.

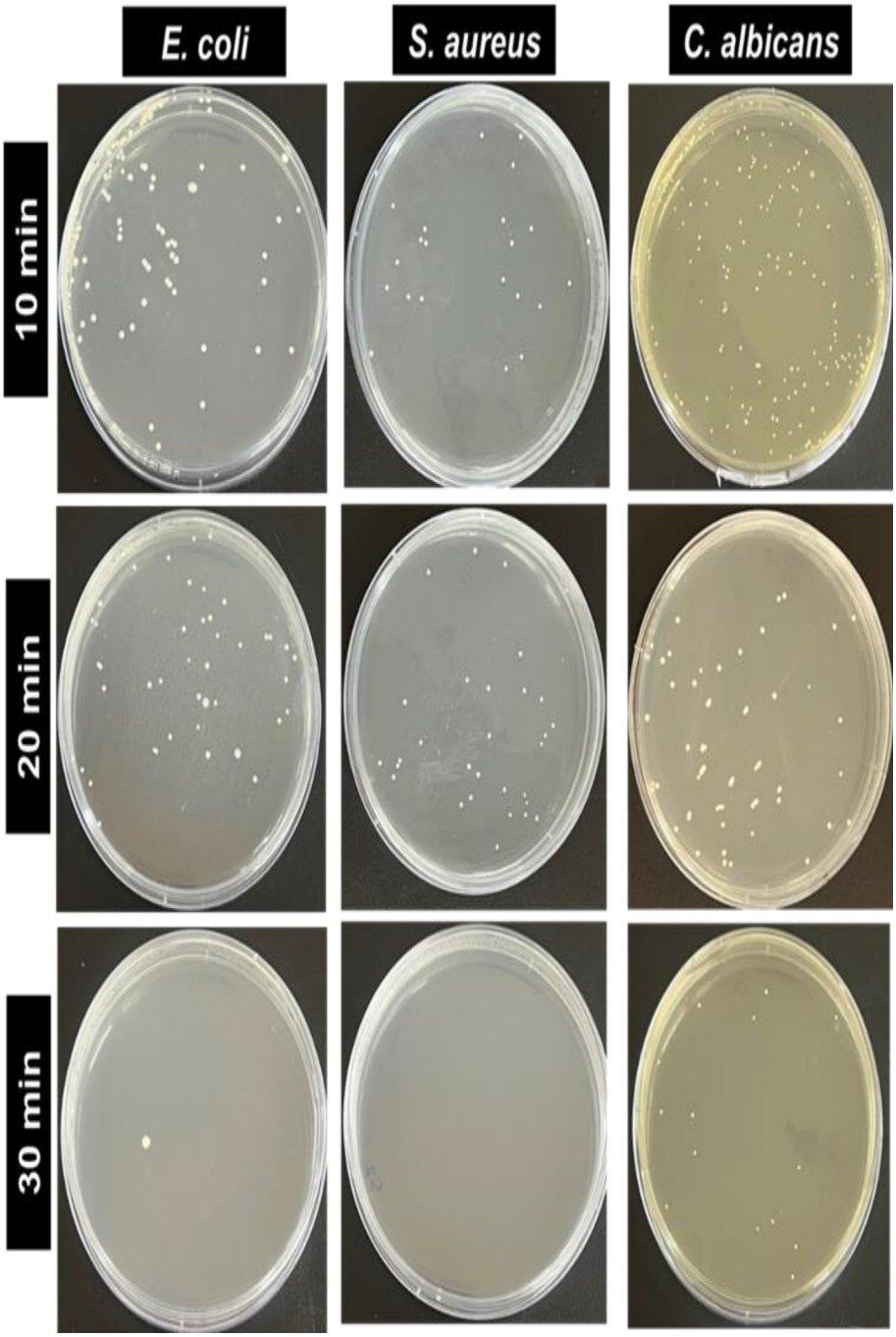

Fig. 12 The photograph of viable *E. coli*, *S. aureus* and *C. albicans* during different UV-irradiation times treated with TiO_2/ZnO bilayer thin film (thermally oxidized at 550 °C).

Table 5 Antimicrobial activity of TiO_2/ZnO sample under various morphology.

Photocatalyst Type	Methods	Disinfection time (min)	Microbial Inhibition (%)			Refs.
			E. coli	*S. aureus*	*C. albicans*	
Nanofiber	Electrospinning	60 min	100	–	–	(Yalcinkaya and Lubasova, 2017)
Nanostructured	Hydrothermal	1440 min	–	51.4	–	(Zhang et al., 2018)
Nanocomposite	Hydrothermal	720 min	89.6	99.5	–	(Pang et al., 2019)
Nanorods	Hydrothermal	240 min	40*	–	–	(Tajdari et al., 2020)
Nanoparticle	Pulsed Laser Ablation	1440 min	~77	~48	–	(Menazea and Awwad, 2020)
Thin Film	MS	60 min, UV	92.7	–	–	(Ton et al., 2020)
Nanocomposites	Solvent thermal	1440 min	86.9	–	–	(Liang et al., 2022)
Thin Film	MS, thermal oxidation	10 min, UV	80.333	82.667	68.333	**This work**
		20 min, UV	87.667	88.833	81.467	
		30 min, UV	97.733	98.066	95.800	

MS (Magnetron Sputtering).
* CFU/mL was calculated from optical density (OD).

4. Conclusions

TiO_2/ZnO bilayer thin films were successfully fabricated using magnetron sputtering and the thermal oxidation method. The oxidation temperature played a role in influencing the structure, optical and photocatalytic properties of TiO_2/ZnO bilayer thin films. ZnO as the bottom layer improves the crystallinity of TiO_2 and prevents the anatase-to-rutile transformation. TiO_2 as the upper layer on ZnO thin films reduces photocorrosion during photodegradation. This study demonstrates that the magnetron sputtering method through the thermal oxidation process can promote the good performance of TiO_2/ZnO bilayer thin films as photocatalysts and antimicrobials. Therefore, TiO_2/ZnO thin films, including UV irradiation lamps, seem to be promising as antimicrobial coatings that are cost and time effective.

CRediT authorship contribution statement

Endrika Widyastuti: Conceptualization, Investigation, Methodology, Visualization, Writing – original draft. **Chen-Tien Chiu:** Data curation, Methodology. **Jue-Liang Hsu:** Supervision, Resources, Funding acquisition, Writing – review & editing. **Ying Chieh Lee:** Conceptualization, Validation, Funding acquisition, Supervision, Writing – review & editing.

Declaration of Competing Interest

The authors declare that they have no known competing financial interests or personal relationships that could have appeared to influence the work reported in this paper.

Acknowledgments

The authors acknowledge Douglas J.H. Shyu and Liyu Chiang from Dept. Biological Science and technology, NPUST, Taiwan, for providing a bacterial culture experiment.

Appendix A. Supplementary material

Supplementary data to this article can be found online at https://doi.org/10.1016/j.arabjc.2023.105010.

References

Abebe, B., Murthy, H.C.A., Amare, E., 2020. Enhancing the photocatalytic efficiency of ZnO: defects, heterojunction, and optimization. Environ. Nanotechnol. Monit. Manage. 14,. https://doi.org/10.1016/j.enmm.2020.100336 100336.

Adams, L.K., Lyon, D.Y., Alvarez, P.J.J., 2006. Comparative ecotoxicity of nanoscale TiO_2, SiO_2, and ZnO water suspensions. Water Res. 40, 3527–3532. https://doi.org/10.1016/j.watres.2006.08.004.

Afreen, G., Shoeb, M., Upadhyayula, S., 2020. Effectiveness of reactive oxygen species generated from rGO/CdS QD heterostructure for photodegradation and disinfection of pollutants in waste water. Mater. Sci. Eng. C 108,. https://doi.org/10.1016/j.msec.2019.110372 110372.

Ahmed, S., Sameen, D.E., Lu, R., Li, R., Dai, J., Qin, W., Liu, Y., 2022. Research progress on antimicrobial materials for food packaging. Crit. Rev. Food Sci. Nutr. 62, 3088–3102. https://doi.org/10.1080/10408398.2020.1863327.

Ali, M.M., Haque, M.J., Kabir, M.H., Kaiyum, M.A., Rahman, M.S., 2021. Nano synthesis of ZnO–TiO_2 composites by sol-gel method and evaluation of their antibacterial, optical and photocatalytic activities. Results Mater. 11,. https://doi.org/10.1016/j.rinma.2021.100199 100199.

Asare, E.O., Mun, E.A., Marsili, E., Paunov, V.N., 2022. Nanotechnologies for control of pathogenic microbial biofilms. J. Mater. Chem. B. https://doi.org/10.1039/d2tb00233g.

Astinchap, B., Moradian, R., Gholami, K., 2017. Effect of sputtering power on optical properties of prepared TiO_2 thin films by thermal oxidation of sputtered Ti layers. Mater. Sci. Semicond. Process. 63, 169–175. https://doi.org/10.1016/j.mssp.2017.02.007.

Ayana, A., Hou, F., Seidel, J., Rajendra, B.V., Sharma, P., 2022. Microstructural and piezoelectric properties of ZnO films. Mater. Sci. Semicond. Process. 146,. https://doi.org/10.1016/j.mssp.2022.106680 106680.

Azizi-Lalabadi, M., Ehsani, A., Divband, B., Alizadeh-Sani, M., 2019. Antimicrobial activity of Titanium dioxide and Zinc oxide nanoparticles supported in 4A zeolite and evaluation the morphological characteristic. Sci. Rep. 9, 1–10. https://doi.org/10.1038/s41598-019-54025-0.

Bouanane, I., Kabir, A., Boulainine, D., Zerkout, S., Schmerber, G., Boudjema, B., 2016. Characterization of ZnO thin films prepared by thermal oxidation of zn. J. Electron. Mater. 45, 3307–3313. https://doi.org/10.1007/s11664-016-4469-6.

Brayner, R., Ferrari-Iliou, R., Brivois, N., Djediat, S., Benedetti, M.F., Fiévet, F., 2006. Toxicological impact studies based on Escherichia coli bacteria in ultrafine ZnO nanoparticles colloidal medium. Nano Lett. 6, 866–870. https://doi.org/10.1021/nl052326h.

Butalid, R.J.B., Cristobal, A.P.S., Montallana, A.D.S., Vasquez Jr, M. R., 2020. Stability of TiO_2-coated ZnO photocatalytic thin films for photodegradation of methylene blue. J. Vac. Sci. Technol., B: Nanotechnol. Microelectron.: Mater., Process., Meas., Phenom. 38, 62205. https://doi.org/10.1116/6.0000306.

Chen, H., Xu, Y., 2014. Photoactivity and stability of Ag_2WO_4 for organic degradation in aqueous suspensions. Appl. Surf. Sci. 319, 319–323. https://doi.org/10.1016/j.apsusc.2014.05.115.

Dhanalakshmi, R., Pandikumar, A., Sujatha, K., Gunasekaran, P., 2013. Photocatalytic and antimicrobial activities of functionalized silicate sol–gel embedded ZnO–TiO_2 nanocomposite materials. Mater. Express 3, 291–300. https://doi.org/10.1166/mex.2013.1133.

El Mragui, A., Daou, I., Zegaoui, O., El Mragui, A., Daou, I., Zegaoui, O., 2019. Influence of the Preparation Method and ZnO/(ZnO+ TiO_2) Weight Ratio on the Physicochemical and Photocatalytic Properties of ZnO-TiO_2 Nanomaterials. Catal. Today 321, 41–51. https://doi.org/10.1016/j.cattod.2018.01.016.

Epand, R.M., Epand, R.F., 2009. Lipid domains in bacterial membranes and the action of antimicrobial agents. Biochimica et Biophysica Acta (BBA)-Biomembranes 1788, 289–294. https://doi.org/10.1016/j.bbamem.2008.08.023.

Espitia, P.J.P., de Soares, N.d.FF., dos Reis Coimbra, J.S., de Andrade, N.J., Cruz, R.S., Medeiros, E.A.A., 2012. Zinc oxide nanoparticles: synthesis, antimicrobial activity and food packaging applications. Food Bioproc Tech. 5, 1447–1464. https://doi.org/10.1007/s11947-012-0797-6.

Firdaus, C.M., Rizam, M.S.B.S., Rusop, M., Hidayah, S.R., 2012. Characterization of ZnO and ZnO: TiO_2 thin films prepared by sol-gel spray-spin coating technique. Procedia Eng. 41, 1367–1373. https://doi.org/10.1016/j.proeng.2012.07.323.

Franklin, N.M., Rogers, N.J., Apte, S.C., Batley, G.E., Gadd, G.E., Casey, P.S., 2007. Comparative toxicity of nanoparticulate ZnO, bulk ZnO, and ZnCl2 to a freshwater microalga (Pseudokirchneriella subcapitata): the importance of particle solubility. Environ. Sci. Tech. 41, 8484–8490. https://doi.org/10.1021/es071445r.

Gordon, T., Perlstein, B., Houbara, O., Felner, I., Banin, E., Margel, S., 2011. Synthesis and characterization of zinc/iron oxide composite nanoparticles and their antibacterial properties. Colloids Surf A Physicochem Eng Asp 374, 1–8. https://doi.org/10.1016/j.colsurfa.2010.10.015.

Güzelçimen, F., Tanören, B., Çetinkaya, Ç., Kaya, M.D., Efkere, H.İ., Özen, Y., Bingöl, D., Sirkeci, M., Kınacı, B., Ünlü, M.B., Özçelik, S., 2020. The effect of thickness on surface structure of rf sputtered TiO_2 thin films by XPS, SEM/EDS, AFM and SAM. Vacuum 182,. https://doi.org/10.1016/j.vacuum.2020.109766 109766.

Harun, N.H., Mydin, R.B.S.M.N., Sreekantan, S., Saharudin, K.A., Khor, Y.L., Basiron, N., Seeni, A., 2018. Antibacterial activity of heterogeneous TiO_2 and ZnO nanoparticles against Gram-positive and Gram-negative bacterial pathogens. J. Biomed. Clin. Sci. (JBCS) 3, 75–78.

Hernández, S., Cauda, V., Hidalgo, D., Rivera, V.F., Manfredi, D., Chiodoni, A., Pirri, F.C., 2014. Fast and low-cost synthesis of 1D ZnO–TiO_2 core–shell nanoarrays: Characterization and enhanced photo-electrochemical performance for water splitting. J. Alloy. Compd. 615, S530–S537. https://doi.org/10.1016/j.jallcom.2014.02.010.

Hussin, R., Seng, G.H., Zulkiflee, N.S., Harun, Z., Hatta, M.N.M., Yunos, M.Z., 2019. ZnO/TiO2 thin films for photocatalytic application. In: AIP Conference Proceedings. AIP Publishing LLC, p. 20096. https://doi.org/10.1063/1.5089395.

Ibrahim, N.B., Al-Shomar, S.M., Ahmad, S.H., 2013. Effect of annealing temperature on the structural and optical properties of nanocrystalline ZnO thin films prepared by sol-gel method. Sains Malays 42, 1781–1786. https://doi.org/10.3740/MRSK.2022.32.5.249.

İkizler, B., Peker, S.M., 2016. Synthesis of TiO_2 coated ZnO nanorod arrays and their stability in photocatalytic flow reactors. Thin Solid Films 605, 232–242. https://doi.org/10.1016/j.tsf.2015.11.083.

Jing, L., Wang, J., Qu, Y., Luan, Y., 2009. Effects of surface-modification with Bi_2O_3 on the thermal stability and photoinduced charge property of nanocrystalline anatase TiO_2 and its enhanced photocatalytic activity. Appl. Surf. Sci. 256, 657–663. https://doi.org/10.1016/j.apsusc.2009.08.037.

Joe, A., Park, S.-H., Shim, K.-D., Kim, D.-J., Jhee, K.-H., Lee, H.-W., Heo, C.-H., Kim, H.-M., Jang, E.-S., 2017. Antibacterial mechanism of ZnO nanoparticles under dark conditions. J. Ind. Eng. Chem. 45, 430–439. https://doi.org/10.1016/j.jiec.2016.10.013.

Kalanur, S.S., Yoo, I.-H., Park, J., Seo, H., 2017. Insights into the electronic bands of WO_3/$BiVO_4$/TiO_2, revealing high solar water splitting efficiency. J. Mater. Chem. A Mater. 5, 1455–1461. https://doi.org/10.1039/c6ta07592d.

Kalarivalappil, V., Vijayan, B.K., Kumar, V., 2019. Engineering nanocrystalline titania thin films for high photocatalytic activity. Mater. Today: Proc. 9, 621–626. https://doi.org/10.1016/j.matpr.2018.10.384.

Kamaruddin, S.A., Chan, K.-Y., Yow, H.-K., Sahdan, M.Z., Saim, H., Knipp, D., 2011. Zinc oxide films prepared by sol–gel spin coating technique. Appl. Phys. A 104, 263–268. https://doi.org/10.1007/s00339-010-6121-2.

Kasemets, K., Ivask, A., Dubourguier, H.-C., Kahru, A., 2009. Toxicity of nanoparticles of ZnO, CuO and TiO_2 to yeast Saccharomyces cerevisiae. Toxicol. In Vitro 23, 1116–1122. https://doi.org/10.1016/j.tiv.2009.05.015.

Khan, M.I., Imran, S., Saleem, M., Rehman, S.U., 2018. Annealing effect on the structural, morphological and electrical properties of TiO_2/ZnO bilayer thin films. Results Phys. 8, 249–252. https://doi.org/10.1016/j.rinp.2017.12.030.

Lachom, V., Poolcharuansin, P., Laokul, P., 2017. Preparation, characterizations and photocatalytic activity of a ZnO/TiO_2 nanocomposite. Mater. Res. Express 4, 35006. https://doi.org/10.1088/2053-1591/aa60d1.

Lee, P.-Y., Widyastuti, E., Lin, T.-C., Chiu, C.-T., Xu, F.-Y., Tseng, Y.-T., Lee, Y.-C., 2021. The phase evolution and photocatalytic properties of a Ti-TiO_2 bilayer thin film prepared using thermal oxidation. Coatings 11, 808. https://doi.org/10.3390/coatings11070808.

Liang, Y., Li, W., Wang, X., Zhou, R., Ding, H., 2022. TiO2–ZnO/Au ternary heterojunction nanocomposite: Excellent antibacterial property and visible-light photocatalytic hydrogen production efficiency. Ceram. Int. 48, 2826–2832. https://doi.org/10.1016/j.ceramint.2021.10.072.

Menazea, A.A., Awwad, N.S., 2020. Antibacterial activity of TiO_2 doped ZnO composite synthesized via laser ablation route for antimicrobial application. J. Mater. Res. Technol. 9, 9434–9441. https://doi.org/10.1016/j.jmrt.2020.05.103.

Mihailova, I., Gerbreders, V., Tamanis, E., Sledevskis, E., Viter, R., Sarajevs, P., 2013. Synthesis of ZnO nanoneedles by thermal oxidation of Zn thin films. J. Non Cryst. Solids 377, 212–216. https://doi.org/10.1016/j.jnoncrysol.2013.05.003.

Munguti, L., Dejene, F., 2020. Influence of annealing temperature on structural, optical and photocatalytic properties of ZnO–TiO_2 composites for application in dye removal in water. Nano-Struct. Nano-Objects 24,. https://doi.org/10.1016/j.nanoso.2020.100594 100594.

Nagvenkar, A.P., Deokar, A., Perelshtein, I., Gedanken, A., 2016. A one-step sonochemical synthesis of stable ZnO–PVA nanocolloid as a potential biocidal agent. J. Mater. Chem. B 4, 2124–2132. https://doi.org/10.1039/C6TB00033A.

Nouasria, F.Z., Selloum, D., Henni, A., Tingry, S., Hrbac, J., 2022. Improvement of the photocatalytic performance of ZnO thin films in the UV and sunlight range by Cu doping and additional coupling

with Cu_2O. Ceram. Int. https://doi.org/10.1016/j.ceramint.2022.01.207.

Pang, S., He, Y., Zhong, R., Guo, Z., He, P., Zhou, C., Xue, B., Wen, X., Li, H., 2019. Multifunctional ZnO/TiO_2 nanoarray composite coating with antibacterial activity, cytocompatibility and piezoelectricity. Ceram. Int. 45, 12663–12671. https://doi.org/10.1016/j.ceramint.2019.03.076.

Parfenova, L.V., Gal'imshina, Z.R., Gilfanova, G.U., Alibaeva, E.I., Danilko, K.V., Pashkova, T.M., Kartashova, O.L., Farrakhov, R. G., Mukaeva, V.R., Parfenov, E.V., 2022. Hyaluronic acid bisphosphonates as antifouling antimicrobial coatings for PEO-modified titanium implants. Surfaces and Interfaces 28. https://doi.org/10.1063/5.0069154.

Pasquet, J., Chevalier, Y., Pelletier, J., Couval, E., Bouvier, D., Bolzinger, M.-A., 2014. The contribution of zinc ions to the antimicrobial activity of zinc oxide. Colloids Surf. A Physicochem. Eng. Asp 457, 263–274. https://doi.org/10.1016/j.colsurfa.2014.05.057.

Pérez-González, M., Tomás, S.A., 2021. Surface chemistry of TiO_2-ZnO thin films doped with Ag. Its role on the photocatalytic degradation of methylene blue. Catal. Today 360, 129–137. https://doi.org/10.1016/j.cattod.2019.08.009.

Pérez-González, M., Tomás, S.A., Morales-Luna, M., Arvizu, M.A., Tellez-Cruz, M.M., 2015. Optical, structural, and morphological properties of photocatalytic TiO_2–ZnO thin films synthesized by the sol–gel process. Thin Solid Films 594, 304–309. https://doi.org/10.1016/j.tsf.2015.04.073.

Pérez-González, M., Tomás, S.A., Santoyo-Salazar, J., Morales-Luna, M., 2017. Enhanced photocatalytic activity of TiO_2-ZnO thin films deposited by dc reactive magnetron sputtering. Ceram. Int. 43, 8831–8838. https://doi.org/10.1016/j.ceramint.2017.04.016.

Phuinthiang, P., Trinh, D.T.T., Channei, D., Ratananikom, K., Sirilak, S., Khanitchaidecha, W., Nakaruk, A., 2021. Novel strategy for the development of antibacterial TiO_2 thin film onto polymer substrate at room temperature. Nanomaterials 11, 1493. https://doi.org/10.3390/nano11061493.

Probst, C., Garcia-Santamarina, S., Brooks, J.T., Van Der Kloet, I., Baars, O., Ralle, M., Thiele, D.J., Alspaugh, J.A., 2022. Interactions between copper homeostasis and the fungal cell wall affect copper stress resistance. PLoS Pathog. 18, e1010195.

Russell, A.D., 2003. Similarities and differences in the responses of microorganisms to biocides. J. Antimicrob. Chemother. 52, 750–763. https://doi.org/10.1093/jac/dkg422.

Rusu, G.G., Gĭrtan, M., Rusu, M., 2007. Preparation and characterization of ZnO thin films prepared by thermal oxidation of evaporated Zn thin films. Superlattice. Microst. 42, 116–122. https://doi.org/10.1016/j.spmi.2007.04.021.

Salaken, S.M., Farzana, E., Podder, J., 2013. Effect of Fe-doping on the structural and optical properties of ZnO thin films prepared by spray pyrolysis. J. Semicond. 34, 73003. https://doi.org/10.1088/1674-4926/34/7/073003.

Sapkal, R.T., Shinde, S.S., Waghmode, T.R., Govindwar, S.P., Rajpure, K.Y., Bhosale, C.H., 2012. Photo-corrosion inhibition and photoactivity enhancement with tailored zinc oxide thin films. J. Photochem. Photobiol. B 110, 15–21. https://doi.org/10.1016/j.jphotobiol.2012.02.004.

Selvamani, V., Kadian, S., Detwiler, D.A., Zareei, A., Woodhouse, I., Qi, Z., Peana, S., Alcaraz, A.M., Wang, H., Rahimi, R., 2022. Laser-Assisted nanotexturing and silver immobilization on titanium implant surfaces to enhance bone cell mineralization and antimicrobial properties. Langmuir 38, 4014–4027. https://doi.org/10.1021/acs.langmuir.2c00008.

Sheridan, M., Winters, C., Zamboni, F., Collins, M.N., 2022. Biomaterials: Antimicrobial surfaces in biomedical engineering and healthcare. Curr Opin Biomed Eng 100373. https://doi.org/10.1016/j.cobme.2022.100373.

Singh, S., Chakrabarti, P., 2013. Optical characterization of ZnO thin films grown by thermal oxidation of metallic zinc. Adv. Sci. Eng. Med. 5, 677–682. https://doi.org/10.1166/asem.2013.1290.

Siwińska-Stefańska, K., Kubiak, A., Piasecki, A., Dobrowolska, A., Czaczyk, K., Motylenko, M., Rafaja, D., Ehrlich, H., Jesionowski, T., 2019. Hydrothermal synthesis of multifunctional TiO_2-ZnO oxide systems with desired antibacterial and photocatalytic properties. Appl. Surf. Sci. 463, 791–801. https://doi.org/10.1016/j.apsusc.2018.08.256.

Sreedhar, A., Jung, H., Kwon, J.H., Yi, J., Sohn, Y., Gwag, J.S., 2017. Novel composite ZnO/TiO_2 thin film photoanodes for enhanced visible-light-driven photoelectrochemical water splitting activity. J. Electroanal. Chem. 804, 92–98. https://doi.org/10.1016/j.jelechem.2017.09.045.

Srinivas, U.S., Tan, B.W.Q., Vellayappan, B.A., Jeyasekharan, A.D., 2019. ROS and the DNA damage response in cancer. Redox Biol. 25,. https://doi.org/10.1016/j.redox.2018.101084 101084.

Suo, X., Zhao, S., Ran, Y., Liu, H., Jiang, Z., Li, Y., Wang, Z., 2019. Effects of oxygen/argon pressure ratio on the structural and optical properties of Mn-doped ZnO thin films prepared by magnetron pulsed co-sputtering. Surf. Coat. Technol. 357, 978–983. https://doi.org/10.1016/j.surfcoat.2018.10.084.

Szeto, H.H., 2006. Cell-permeable, mitochondrial-targeted, peptide antioxidants. AAPS J. 8, E277–E283. https://doi.org/10.1007/BF02854898.

Tajdari, A., Babaei, A., Goudarzi, A., Partovi, R., 2020. Preparation and study on the optical, mechanical, and antibacterial properties of polylactic acid/ZnO/TiO_2 shared nanocomposites. J. Plast. Film Sheeting 36, 285–311. https://doi.org/10.1177/8756087919900365.

Tekin, D., Kiziltas, H., Ungan, H., 2020. Kinetic evaluation of ZnO/TiO_2 thin film photocatalyst in photocatalytic degradation of Orange G. J. Mol. Liq. 306,. https://doi.org/10.1016/j.molliq.2020.112905 112905.

Ting, C.-C., Chen, S.-Y., Liu, D.-M., 2000. Structural evolution and optical properties of TiO_2 thin films prepared by thermal oxidation of sputtered Ti films. J. Appl. Phys. 88, 4628–4633. https://doi.org/10.1063/1.1309039.

Ton, N.Q.T., Le, T.N.T., Kim, S., Dao, V.A., Yi, J., Vu, T.H.T., 2020. High-efficiency photo-generated charges of ZnO/TiO_2 heterojunction thin films for photocatalytic and antibacterial performance. J. Nanosci. Nanotechnol. 20, 2214–2222. https://doi.org/10.1166/jnn.2020.17306.

Vignesh, K., Vijayalakshmi, K.A., Karthikeyan, N., 2017. Sol-gel synthesis and antibacterial study on BC/ZnO/TiO_2 nanocomposite treated by DC glow discharge plasma. J. Adhes. Sci. Technol. 31, 1075–1086. https://doi.org/10.1080/01694243.2016.1244036.

Vinu, R., Madras, G., 2010. Environmental remediation by photocatalysis. J. Indian Inst. Sci. 90, 189–230.

Widyastuti, E., Xu, F.-Y., Chiu, C.-T., Jan, J.-H., Hsu, J.-L., Lee, Y.-C., 2021. A study on the characteristic and antibacterial activity of Ti_3Ox thin films. Catalysts 11, 1416. https://doi.org/10.3390/catal11111416.

Widyastuti, E., Hsu, J.-L., Lee, Y.-C., 2022. Insight on photocatalytic and photoinduced antimicrobial properties of ZnO thin films deposited by HiPIMS through thermal oxidation. Nanomaterials 12, 463. https://doi.org/10.3390/nano12030463.

Wittawat, R., Rittipun, R., Jarasfah, M., Nattaporn, B., 2020. Synthesis of ZnO/TiO_2 spherical particles for blue light screening by ultrasonic spray pyrolysis. Mater. Today Commun. 24,. https://doi.org/10.1016/j.mtcomm.2020.101126 101126.

Yalcinkaya, F., Lubasova, D., 2017. Quantitative evaluation of antibacterial activities of nanoparticles (ZnO, TiO_2, ZnO/TiO_2, SnO_2, CuO, ZrO_2, and $AgNO_3$) incorporated into polyvinyl butyral nanofibers. Polym. Adv. Technol. 28, 137–140. https://doi.org/10.1002/pat.3883.

Yan, X., Zou, C., Gao, X., Gao, W., 2012. ZnO/TiO 2 core–brush nanostructure: processing, microstructure and enhanced photocat-

alytic activity. J. Mater. Chem. 22, 5629–5640. https://doi.org/10.1039/c2jm15477c.

Yeh, J., Chen, S., Lin, S., Gan, J., Chin, T., Shun, T., Tsau, C., Chang, S., 2004. Nanostructured high-entropy alloys with multiple principal elements: novel alloy design concepts and outcomes. Adv. Eng. Mater. 6, 299–303.

Yeh, M.-Y., Lee, P.-Y., Shang, J.-T., Lee, Y.-C., 2018. Effect of thermal oxidation temperatures on the phase evolution and photocatalytic property of tungsten-doped TiO_2 thin film. Jpn. J. Appl. Phys. 57,. https://doi.org/10.7567/JJAP.57.125801 125801.

Yemmireddy, V.K., Hung, Y., 2017. Using photocatalyst metal oxides as antimicrobial surface coatings to ensure food safety—Opportunities and challenges. Compr. Rev. Food Sci. Food Saf. 16, 617–631. https://doi.org/10.1111/1541-4337.12267.

Yu, Y., Yao, B., He, Y., Cao, B., Ma, W., Chang, L., 2020. Oxygen defect-rich In-doped ZnO nanostructure for enhanced visible light photocatalytic activity. Mater. Chem. Phys. 244,. https://doi.org/10.1016/j.matchemphys.2020.122672 122672.

Zhang, L., Ding, Y., Povey, M., York, D., 2008. ZnO nanofluids–A potential antibacterial agent. Prog. Nat. Sci. 18, 939–944. https://doi.org/10.1016/j.pnsc.2008.01.026.

Zhang, R., Liu, X., Xiong, Z., Huang, Q., Yang, X., Yan, H., Ma, J., Feng, Q., Shen, Z., 2018. Novel micro/nanostructured TiO_2/ZnO coating with antibacterial capacity and cytocompatibility. Ceram. Int. 44, 9711–9719. https://doi.org/10.1016/j.ceramint.2018.02.202.

Zhou, B., Jiang, X., Liu, Z., Shen, R., Rogachev, A.V., 2013a. Preparation and characterization of TiO_2 thin film by thermal oxidation of sputtered Ti film. Mater. Sci. Semicond. Process. 16, 513–519. https://doi.org/10.1016/j.mssp.2012.05.001.

Zhou, Y., Yang, L., Huang, Y., 2013b. Micro-and macromechanical properties of materials. CRC Press.

Zhou, Y., Tan, Y., Xiang, Y., Zhu, J., 2019. Construction of Urchin-Like ZnO/TiO2 Direct Z-Scheme System to Improve Charge Separation. ChemistrySelect 4, 12963–12970. https://doi.org/10.1002/slct.201903905.

Zhu, S., Li, L., Liu, J., Wang, H., Wang, T., Zhang, Y., Zhang, L., Ruoff, R.S., Dong, F., 2018. Structural directed growth of ultrathin parallel birnessite on β-MnO_2 for high-performance asymmetric supercapacitors. ACS Nano 12, 1033–1042. https://doi.org/10.1021/acsnano.7b03431.